AMERICAN SOCIETY FOR MICROBIOLOGY | Journal of Virology®

VIRUS-CELL INTERACTIONS

Experimental Adaptive Evolution of Simian Immunodeficiency Virus SIVcpz to Pandemic Human Immunodeficiency Virus Type 1 by Using a Humanized Mouse Model

Kei Sato,[a,b,c] Naoko Misawa,[a,b] Junko S. Takeuchi,[a*] Tomoko Kobayashi,[a*] Taisuke Izumi,[a,b*] Hirofumi Aso,[b,d] Shumpei Nagaoka,[b,e] Keisuke Yamamoto,[b,f] Izumi Kimura,[b,g] Yoriyuki Konno,[b,e] Yusuke Nakano,[a,b] Yoshio Koyanagi[a,b]

[a]Laboratory of Viral Pathogenesis, Institute for Virus Research, Kyoto University, Kyoto, Japan
[b]Laboratory of Systems Virology, Department of Biosystems Science, Institute for Frontier Life and Medical Sciences, Kyoto University, Kyoto, Japan
[c]CREST, Japan Science and Technology Agency, Saitama, Japan
[d]Faculty of Pharmaceutical Sciences, Kyoto University, Kyoto, Japan
[e]Graduate School of Biostudies, Kyoto University, Kyoto, Japan
[f]Graduate School of Medicine, Kyoto University, Kyoto, Japan
[g]Graduate School of Pharmaceutical Sciences, Kyoto University, Kyoto, Japan

ABSTRACT Human immunodeficiency virus type 1 (HIV-1), the causative agent of AIDS, originated from simian immunodeficiency virus from chimpanzees (SIVcpz), the precursor of the human virus, approximately 100 years ago. This indicates that HIV-1 has emerged through the cross-species transmission of SIVcpz from chimpanzees to humans. However, it remains unclear how SIVcpz has evolved into pandemic HIV-1 in humans. To address this question, we inoculated three SIVcpz strains (MB897, EK505, and MT145), four pandemic HIV-1 strains (NL4-3, NLCSFV3, JRCSF, and AD8), and two nonpandemic HIV-1 strains (YBF30 and DJO0131). Humanized mice infected with SIVcpz strain MB897, a virus phylogenetically similar to pandemic HIV-1, exhibited a peak viral load comparable to that of mice infected with pandemic HIV-1, while peak viral loads of mice infected with SIVcpz strain EK505 or MT145 as well as nonpandemic HIV-1 strains were significantly lower. These results suggest that SIVcpz strain MB897 is preadapted to humans, unlike the other SIVcpz strains. Moreover, viral RNA sequencing of MB897-infected humanized mice identified a nonsynonymous mutation in *env*, a G413R substitution in gp120. The infectivity of the gp120 G413R mutant of MB897 was significantly higher than that of parental MB897. Furthermore, we demonstrated that the gp120 G413R mutant of MB897 augments the capacity for viral replication in both *in vitro* cell cultures and humanized mice. Taken together, this is the first experimental investigation to use an animal model to demonstrate a gain-of-function evolution of SIVcpz into pandemic HIV-1.

IMPORTANCE From the mid-20th century, humans have been exposed to the menace of infectious viral diseases, such as severe acute respiratory syndrome coronavirus, Ebola virus, and Zika virus. These outbreaks of emerging/reemerging viruses can be triggered by cross-species viral transmission from wild animals to humans, or zoonoses. HIV-1, the causative agent of AIDS, emerged by the cross-species transmission of SIVcpz, the HIV-1 precursor in chimpanzees, around 100 years ago. However, the process by which SIVcpz evolved to become HIV-1 in humans remains unclear. Here, by using a hematopoietic stem cell-transplanted humanized-mouse model, we experimentally recapitulate the evolutionary process of SIVcpz to become HIV-1. We provide evidence suggesting that a strain of SIVcpz, MB897, preadapted to infect humans over other SIVcpz strains. We further demonstrate a gain-of-function evolution of SIVcpz in infected humanized mice.

Received 1 November 2017 **Accepted** 28 November 2017

Accepted manuscript posted online 6 December 2017

Citation Sato K, Misawa N, Takeuchi JS, Kobayashi T, Izumi T, Aso H, Nagaoka S, Yamamoto K, Kimura I, Konno Y, Nakano Y, Koyanagi Y. 2018. Experimental adaptive evolution of simian immunodeficiency virus SIVcpz to pandemic human immunodeficiency virus type 1 by using a humanized mouse model. J Virol 92:e01905-17. https://doi.org/10.1128/JVI.01905-17.

Editor Frank Kirchhoff, Ulm University Medical Center

Address correspondence to Kei Sato, ksato@virus.kyoto-u.ac.jp.

* Present address: Junko S. Takeuchi, Department of Virology II, National Institute of Infectious Diseases, Tokyo, Japan; Tomoko Kobayashi, Laboratory of Animal Health, Department of Animal Science, Faculty of Agriculture, Tokyo University of Agriculture, Atsugi, Kanagawa, Japan; Taisuke Izumi, Frederick National Laboratory for Cancer Research, Frederick, Maryland, USA.

Our study reveals that pandemic HIV-1 has emerged through at least two steps: preadaptation and subsequent gain-of-function mutations.

KEYWORDS HIV-1, SIVcpz, cross-species transmission, humanized mouse, viral evolution

Humans are susceptible to the threat of emerging/reemerging infectious diseases, which are usually caused by viruses. For instance, West African countries recently suffered from an outbreak of Ebola virus in 2014 to 2015 (1–5). These outbreaks are examples of emerging viruses that can be transferred from animals to humans via cross-species transmission or zoonosis. In fact, it has been estimated that approximately 60% of emerging infectious diseases originate as zoonoses and that the majority (71.8%) are brought from wildlife (6).

For successful cross-species transmission, pathogens must overcome several hurdles to infect a new host species, as they must (i) be encountered by, exposed to, and transferred to the host; (ii) be taken up by the host; (iii) establish infection in the host; (iv) fully adapt to and propagate within the host through acquiring mutations (if needed); and finally, (v) be able to transmit efficiently between the hosts of the new species (for reviews, see references 7 to 9). AIDS, caused by infection with human immunodeficiency virus type 1 (HIV-1), emerged in the 20th century as one of the worst infectious diseases (10, 11). Previous studies have reported that HIV-1 emerged through the cross-species transmission of simian immunodeficiency virus (SIV) in Central African chimpanzees (*Pan troglodytes troglodytes*) (SIVcpz*Ptt*) to humans (12–17). Only two SIVcpz*Ptt* viruses have successfully invaded the human population: HIV-1 group M (for "major" or "main"; HIV-1M) and group N (for "new" or "non-M"; HIV-1N) (12). The limited number of chimpanzee-to-human cross-species transmission events implies that certain factors have affected the efficiency/probability with which SIVcpz*Ptt* infects humans. Moreover, although over 70 million people have been infected with HIV-1M thus far, indicating a pandemic (UNAIDS, WHO; http://www.unaids.org), fewer than 20 patients, mainly in Cameroon, have been reported as infected with HIV-1N (18, 19). However, how certain SIVcpz*Ptt* viruses succeeded in the chimpanzee-to-human transmission and how HIV-1M was established as a pandemic pathogen in the decades immediately following its transfer to humans remain largely unknown.

Cellular antiviral proteins called restriction factors play pivotal roles as species-specific barriers to cross-species viral transmission and limit viral spread into new hosts (20). A series of restriction factors have been identified in primate lentivirus infections, including APOBEC3 (apolipoprotein B mRNA-editing enzyme, catalytic polypeptide-like 3) (21) and tetherin (also known as bone marrow stromal antigen 2 [BST2]) (22, 23). To overcome the species-specific barriers mediated by host proteins, primate lentiviruses have evolutionarily acquired mechanisms of overcoming these restriction factors. Viral infectivity factor (Vif) counteracts the antiviral actions of APOBEC3 proteins (e.g., APOBEC3F and APOBEC3G), while viral protein U (Vpu) and/or negative factor (Nef) antagonizes tetherin-mediated antiviral effect (for reviews, see references 24 to 27). Particularly, the Vpu of HIV-1M, but not those of SIVcpz or the other types of HIV-1, antagonizes human tetherin (28–30), suggesting that the Vpu-mediated antitetherin ability is crucial for increasing viral fitness and the efficiency of human-to-human viral spread (31). However, although SIVcpz*Ptt* is partially capable of replicating in human tissue cultures (32) and a humanized-mouse model (33), the process by which SIVcpz*Ptt* evolved to become HIV-1 in humans remains unclear. Moreover, although a recent study by Yuan et al. used a bone marrow/liver/thymus (BLT)– humanized-mouse model for SIVcpz infection and detected a nonsynonymous mutation in *env* in SIVcpz-infected humanized mice (33), the virological significance of this mutation has not been addressed.

To recapitulate and characterize HIV-1 replication and pathogenesis that occurs naturally in humans, we have established an *in vivo* model of human hematopoietic stem cell-transplanted humanized mice (34–37). The humanized mice are able to

reproduce the characteristics of HIV-1 pathogenesis in humans, such as the gradual decrease of peripheral human CD4$^+$ T cells (34–37). Moreover, we previously investigated the interplay between viral and host proteins involved with viral replication in this mouse model (37–42). Here, we further employ this humanized-mouse model to experimentally reproduce the adaptive evolutionary process of SIVcpz*Ptt* to infect humans. First, we show that the replication efficacy of SIVcpz*Ptt* strain MB897, which is phylogenetically closest to HIV-1M, is significantly higher than those of the other SIVcpz*Ptt* strains in humanized mice, particularly during the initial phase of infection. Moreover, we detected a nonsynonymous mutation, G413R, in the *env* gene of SIVcpz*Ptt* strain MB897 from infected humanized mice and demonstrate that the G413R mutation increases viral fitness *in vitro* and *in vivo* by augmenting viral infectivity. This is the first investigation to experimentally demonstrate the dynamics of the cross-species, adaptive evolution of SIVcpz to infect humans using an animal model.

RESULTS

Preadaptation of SIVcpz*Ptt* in humanized mice. To investigate the evolution of SIVcpz, we included in our study four strains of HIV-1M (strains NL4-3, NLCSFV3, JRCSF, and AD8), two strains of HIV-1N (strains YBF30 and DJO0131), and three strains of SIVcpz*Ptt* (strains MB897, EK505, and MT145). Figure 1A illustrates a phylogenetic tree of HIV-1 and SIVcpz strains, and some of their characteristics are summarized in Fig. 1B (similarities between these viruses are also summarized in Fig. 1D). As previously reported (12, 32, 43), SIVcpz*Ptt* MB897 and EK505 are phylogenetically similar to HIV-1M and HIV-1N, respectively, while there are no HIV-1 strains related to SIVcpz*Ptt* MT145 (Fig. 1A). Infectious molecular clones (IMCs) of these viruses, except for HIV-1N YBF30, were transfected into human embryonic kidney 293T (HEK293T) cells, and the supernatant, containing virus, was collected for use in subsequent experiments. A preparation of HIV-1N YBF30 was prepared by expanding the virus in a culture of phytohemagglutinin (PHA)-activated human peripheral blood mononuclear cells (PBMCs). As shown in Fig. 1C, TZM-bl indicator cells were used to measure viral infectivity, which demonstrated that HIV-1N and SIVcpz*Ptt* strains had infectivities comparable to those of HIV-1M strains and that the infectivity of SIVcpz*Ptt* MB897 was lowest among the SIVcpz*Ptt* strains.

Humanized mice were inoculated with the virus preparations, and then the viral RNA (vRNA) in the plasma and the number of human CD4$^+$ T cells (determined as CD45$^+$ CD3$^+$ CD4$^+$ cells) in the peripheral blood (PB) were longitudinally monitored until 15 weeks postinfection (wpi). As shown in Fig. 2A, the vRNA levels of the mice infected with either the HIV-1N or the SIVcpz*Ptt* strain were significantly lower than those of mice infected with one of the HIV-1M strains. Although HIV-1M-infected mice showed a gradual and significant decrease in the number of peripheral human CD4$^+$ T cells compared to that of mock-infected mice, the mice infected with either an HIV-1N or an SIVcpz*Ptt* strain maintained relatively constant numbers of these cells. A partial decrease in the number of peripheral CD4$^+$ T cells was observed in SIVcpz*Ptt* MB897-infected mice after 12 wpi (Fig. 2B). These findings suggest that the viral replication capacity and pathogenicity of HIV-1M strains are greater than those of the other viruses, including HIV-1N and SIVcpz*Ptt* strains, in a humanized-mouse model.

To further explore the characteristics of viral replication and pathogenicity, we longitudinally assessed vRNA until 15 wpi. As shown in Fig. 2C, mice infected with each of the four HIV-1M strains, two HIV-1N strains, or SIVcpz*Ptt* MB897 had similar maximum vRNA levels ($P = 0.25$ by the Kruskal-Wallis test), while the maximum vRNA level in SIVcpz*Ptt* EK505-infected mice was significantly lower than those of HIV-1M- and SIVcpz*Ptt* MB897-infected mice. In addition, although a significant proportion of virus-producing (i.e., Gag-positive) cells were found in the spleens of infected mice at 15 wpi, the proportions did not differ depending on the type of virus used for inoculation (Fig. 2D). Unlike with the PB (Fig. 2B), significant decreases in the number of splenic human CD4$^+$ T cells were observed in all infected mice at 15 wpi (Fig. 2E). Moreover, it was of

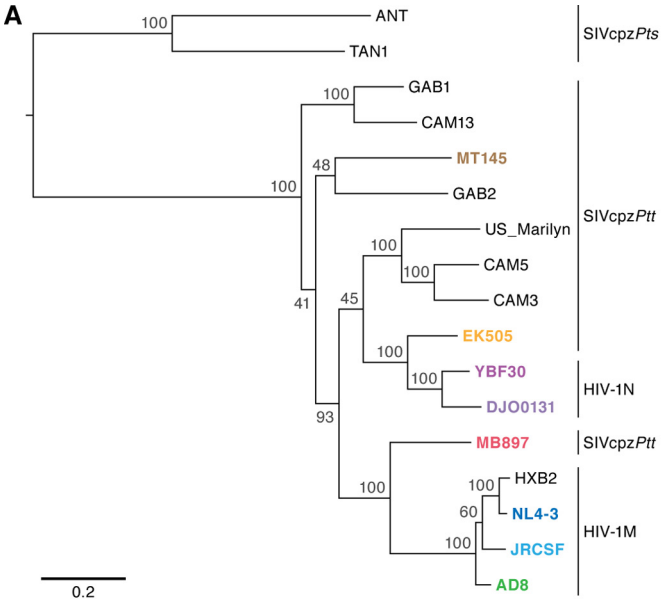

B

Virus	Strain	Coreceptor usage	Source	Accession no.
HIV-1M	NL4-3	CXCR4	Laboratory clone	M19921
	NLCSFV3	CCR5	Contains V3 of JRCSF	NA
	JRCSF	CCR5	Cerebrospinal fluid	M38429
	AD8	CCR5	Laboratory clone	AF004394
HIV-1N	YBF30	CCR5	PBMC proviral DNA	AJ006022
	DJO0131	CCR5	Plasma viral RNA	AY532635
SIVcpz*Ptt*	MB897	CCR5	Fecal viral RNA	JN835461
	EK505	CCR5	Fecal viral RNA	JN835460
	MT145	CCR5	Fecal viral RNA	JN835462

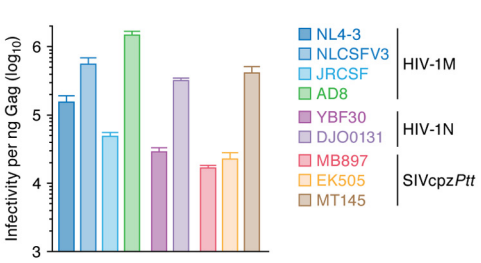

D

Virus	Strain	% Similarity to:								
		NL4-3	JRCSF	AD8	YBF30	DJO0131	MB897	EK505	MT145	GAB1
HIV-1M	JRCSF	94.0								
	AD8	92.2	92.3							
HIV-1N	YBF30	61.0	59.0	61.1						
	DJO0131	60.6	58.1	58.0	88.8					
SIVcpz*Ptt*	MB897	66.3	67.2	66.4	63.2	62.6				
	EK505	60.4	60.7	61.8	79.7	78.7	65.8			
	MT145	56.9	57.1	59.4	63.8	62.6	37.8	63.6		
	GAB1	59.2	61.3	62.4	46.7	54.7	61.4	61.6	59.8	
SIVcpz*Pts*	TAN1	47.3	41.5	47.5	44.9	45.8	45.2	48.5	47.1	44.1

FIG 1 Evolutionary relationship of HIV-1 and SIVcpz. (A) Phylogenetic tree of HIV-1 and SIVcpz. The amino acid sequences of nine viral proteins (Gag, Pol, Vif, Vpr, Tat, Rev, Vpu, Env, and Nef) were concatenated and aligned as described in Materials and Methods. The GenBank accession numbers of the HIV/SIVcpz sequences used in this analysis are listed in Table 3. The tree was constructed using the maximum-likelihood method. Bootstrap values are represented on each node. The virus strains used in this study are shown in bold in individual colors. The scale bar indicates 0.2 amino acid substitutions per site. *Ptt*, *Pan troglodytes troglodytes*; *Pts*, *Pan troglodytes schweinfurthii*. (B) HIV-1 and SIVcpz used in this study. NA, not applicable (71). The Env V3 region of NL4-3 was swapped with that of JRCSF. (C) TZM-bl cell assay. One microgram of each IMC, except for YBF30, was transfected into HEK293T cells. Forty-eight hours posttransfection, the culture supernatant was harvested as virus supernatant (for more detail, see Materials and Methods). The amount of viral particles was quantified by p24 ELISA, and the infectivity of each virus was determined using the TZM-bl cell assay. The assay was performed in triplicate, and averages with SDs are shown. The virus supernatant of YBF30 was prepared as described in Materials and Methods. (D) The percentages of similarity between the viruses are summarized.

interest that the level of acute vRNA of SIVcpz*Ptt* MB897 was comparable to those of HIV-1M strains ($P = 0.20$ by the Mann-Whitney U test) and was significantly higher than those of HIV-1N strains ($P = 0.0086$ by the Mann-Whitney U test) and the other two SIVcpz*Ptt* strains ($P = 0.0086$ versus EK505; $P = 0.0077$ versus MT145) (Fig. 2F).

Next, we assessed each of the aforementioned parameters for correlation with viral replication capacity and/or pathogenicity using the nonparametric Spearman rank correlation test. Notably, two of the parameters, acute vRNA and minimum $CD4^+$ T cell numbers in PB, were significantly correlated using this method (Fig. 3A). Additionally, SIVcpz*Ptt* MB897 displayed parameters similar to those of strains of HIV-1M (Fig. 3B and C). Taken together, these data indicate that the replication capacity and pathogenicity of SIVcpz*Ptt* MB897 are more similar to those of HIV-1M strains than those of the other SIVcpz*Ptt* strains tested (EK505 and MT145). These results further suggest that SIVcpz*Ptt* MB897 has preadapted to infect humans relatively more than the other SIVcpz*Ptt* strains.

***De novo* mutations of SIVcpz*Ptt* in humanized mice.** To address whether SIVcpz*Ptt* viruses acquired some mutations in infected humanized mice, we analyzed the full-length sequence of vRNA in the plasma of SIVcpz*Ptt*-infected mice at

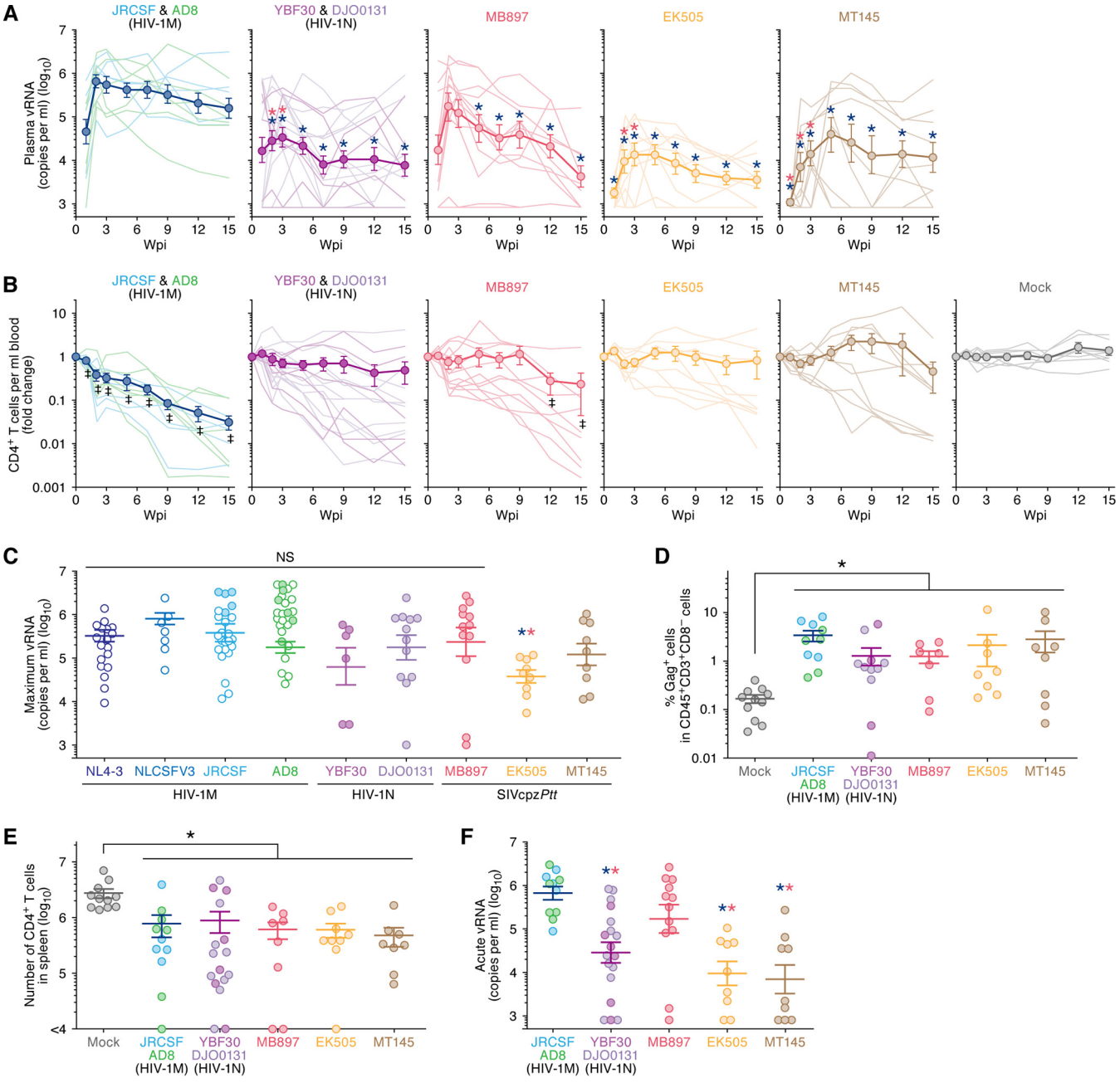

FIG 2 Dynamics of SIVcpz*Ptt* infection in humanized mice. (A and B) The virus supernatants containing 5 ng of p24 antigen (from HIV-1M JRCSF [$n = 5$], HIV-1M AD8 [$n = 6$], HIV-1N YBF30 [$n = 6$], HIV-1N DJO0131 [$n = 12$], SIVcpz*Ptt* MB897 [$n = 10$], SIVcpz*Ptt* EK505 [$n = 9$], and SIVcpz*Ptt* MT145 [$n = 7$]) or RPMI 1640 ($n = 8$; for mock infection) were inoculated into humanized mice, and the amount of vRNA in the plasma (A) and the level of peripheral human $CD4^+$ T cells ($CD45^+$ $CD3^+$ $CD4^+$ cells) (B) were analyzed at 0, 1, 2, 3, 5, 7, 9, 12, and 15 wpi. Each average with SEM is shown as a dot with an error bar, and the values from each mouse are shown by lines. *x* axes, numbers of weeks postinfection. (A) The detection limit of HIV-1 RNA is 800 copies/ml plasma. (C to F) Virological features of infected mice at 15 wpi. (C and F) Maximum vRNA by 15 wpi (C) and acute vRNA (i.e., vRNA at 2 wpi) (F) are shown. The values from each infected mouse are shown by dots. The horizontal bars represent averages with SEMs. (C) Filled dots represent the results newly obtained in this study, while open dots in the HIV-1M section (strains NL4-3, NLCSFV3, JRCSF, and AD8) represent the results from our previous studies (34, 38–41). (D and E) Dynamics of SIVcpz*Ptt* infection in the spleens of humanized mice. (D) The levels of virus-infected cells (i.e., Gag-positive cells) in the spleens of mice infected with HIV-1M JRCSF ($n = 5$), HIV-1M AD8 ($n = 5$), HIV-1N YBF30 ($n = 4$), HIV-1N DJO0131 ($n = 7$), SIVcpz*Ptt* MB897 ($n = 7$), SIVcpz*Ptt* EK505 ($n = 8$), and SIVcpz*Ptt* MT145 ($n = 8$) and of mock-infected mice ($n = 11$) were analyzed by flow cytometry. (E) The numbers of human $CD4^+$ T cells in the spleens of mice infected with HIV-1M JRCSF ($n = 5$), HIV-1M AD8 ($n = 6$), HIV-1N YBF30 ($n = 6$), HIV-1N DJO0131 ($n = 10$), SIVcpz*Ptt* MB897 ($n = 8$), SIVcpz*Ptt* EK505 ($n = 9$), and SIVcpz*Ptt* MT145 ($n = 8$) and of mock-infected mice ($n = 11$) were analyzed by flow cytometry. (A to C and F) Statistically significant differences were determined with the Mann-Whitney U test and are represented as follows: double dagger, *P* was <0.05 versus mock-infected mice; blue asterisk, *P* was <0.05 versus HIV-1M; and red asterisk, *P* was <0.05 versus SIVcpz*Ptt* MB897. (D and E) Asterisks indicate statistically significant differences ($P < 0.05$ by the Mann-Whitney U test) from mock-infected mice. NS, no statistical significance.

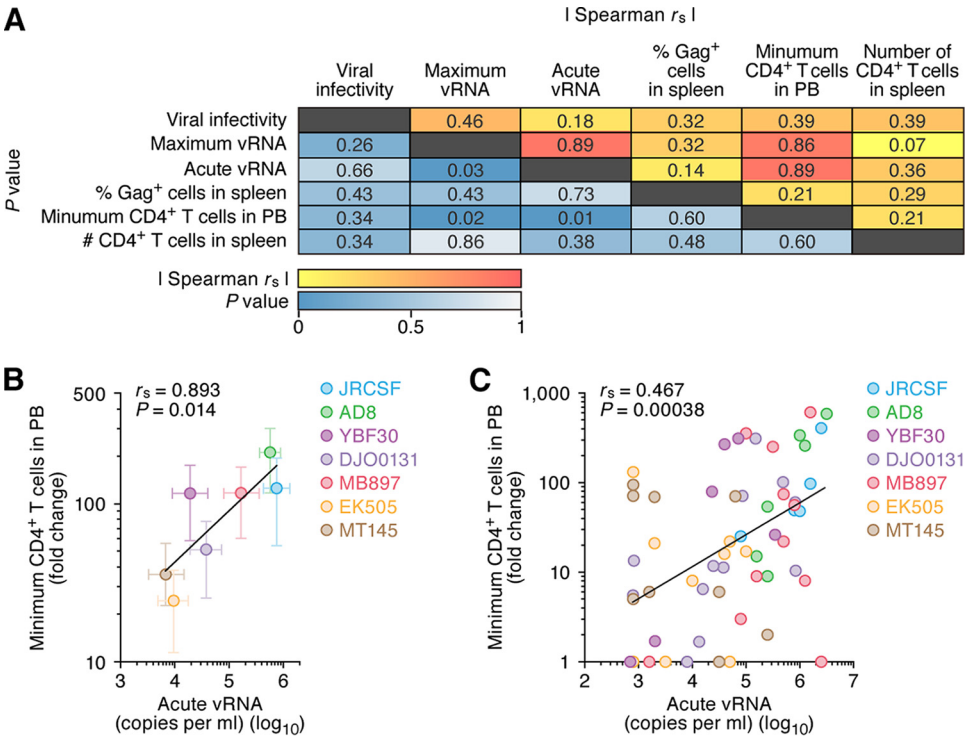

FIG 3 Correlation between acute vRNA and CD4$^+$ T cell decrease. (A) Correlation between virological parameters. The statistical values (*P* values and the absolute values of Spearman's rank correlation coefficient [r_s]) between the two virological parameters shown in Fig. 1C and 2 are summarized. (B and C) Correlation between acute vRNA level and CD4$^+$ T cell decrease. The minimum CD4$^+$ T cell decrease by 15 wpi (*y* axes) and acute vRNA level (i.e., plasma vRNA at 2 wpi) (*x* axes) are shown. The averages with SEMs (B) and the result from each mouse infected with HIV-1M AD8 ($n = 6$), HIV-1N YBF30 ($n = 6$), HIV-1N DJO0131 ($n = 12$), SIVcpz*Ptt* MB897 ($n = 10$), SIVcpz*Ptt* EK505 ($n = 9$), and SIVcpz*Ptt* MT145 ($n = 7$) (C) are shown. The lines represent exponential approximation. Spearman's rank correlation coefficient (r_s) was adopted to determine a statistically significant correlation between each value.

15 wpi. As shown in Fig. 4A, certain mutations were detected in all SIVcpz*Ptt*-infected mice. For instance, some nonsynonymous mutations were detected in the regions encoding Vif (Fig. 4A). However, consistently with previous studies (44–46), the Vif proteins of SIVcpz*Ptt* strains used in this study were efficiently capable of counteracting human APOBEC3F and APOBEC3G (Fig. 4B). These results suggest that no mutations are required for SIVcpz*Ptt* Vif to degrade antiviral human APOBEC3 proteins *in vivo*.

As shown in Fig. 4A (indicated with a red asterisk), all SIVcpz*Ptt* MB897-infected mice exhibited a common mutation in the region encoding Env. This nonsynonymous mutation is G7032A at the nucleotide level, which corresponds to the glycine (G) positioned at amino acid 413 of gp120 being replaced with arginine (R) (gp120 G413R). This residue is located in the C4 region of gp120, and a structure homology model of SIVcpz*Ptt* MB897 gp120 predicted that this residue is exposed on the surface of the protein (Fig. 4C).

The gp120 G413R mutation was found in all three SIVcpz*Ptt* MB897-infected mice analyzed (Fig. 4A) and in a previous study by Yuan et al. (33). Therefore, we assumed a benefit of this nonsynonymous mutation for virus infection. To address this hypothesis, we prepared an IMC of SIVcpz*Ptt* MB897 with the G413R mutation and then assessed its infectivity using the TZM-bl cell assay. Notably, the infectivity of the virus containing the gp120 G413R mutation was significantly (approximately 3.9-fold) higher than that of the parental virus (Fig. 4D), suggesting that the G413R substitution is advantageous for SIVcpz*Ptt* MB897 in infecting humans.

Importance of augmenting infectivity and the ability to antagonize tetherin *in vitro* and *in vivo*. To investigate the effect of mutation/evolution in SIVcpz*Ptt* on its

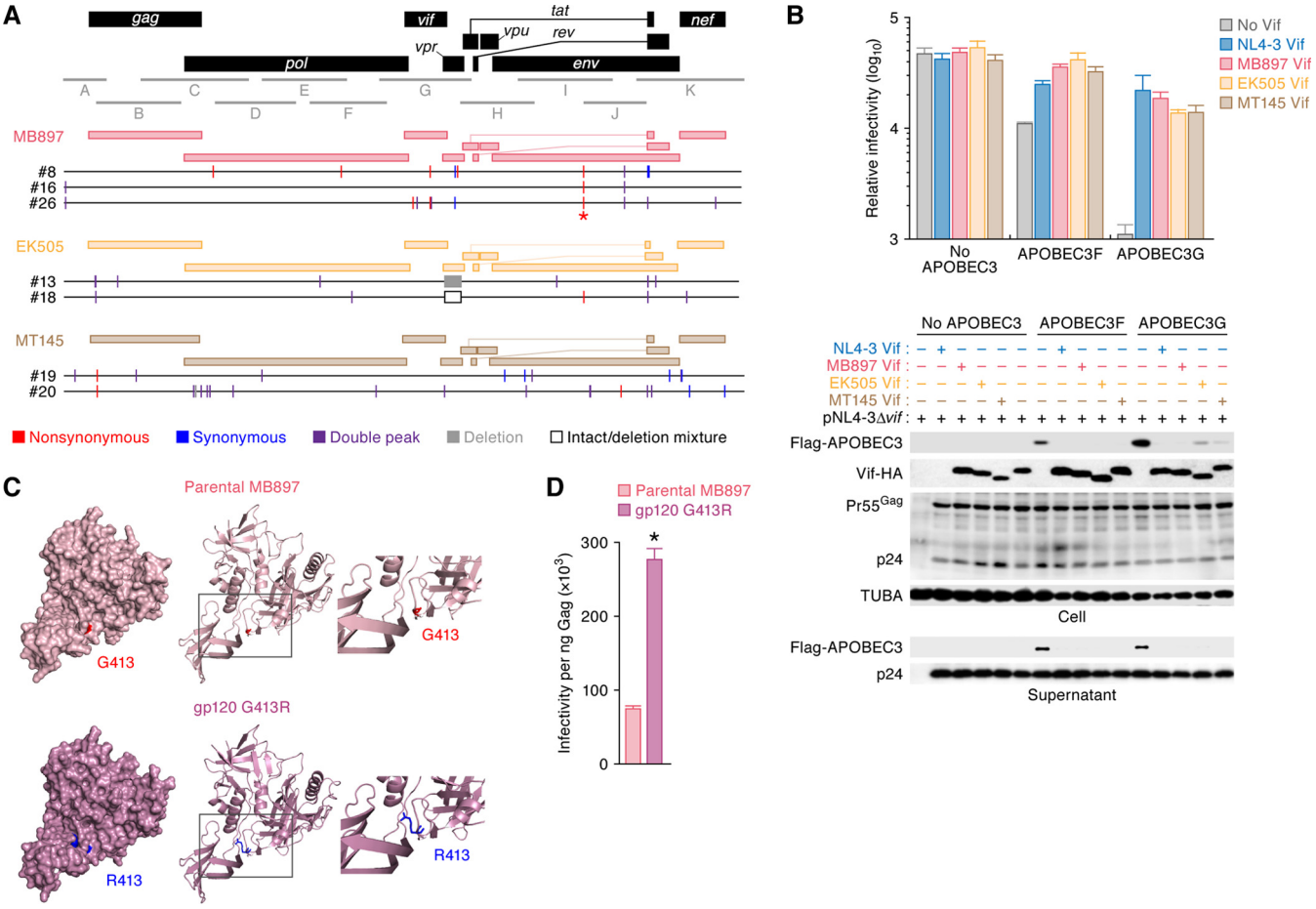

FIG 4 Emergence of SIVcpz*Ptt* derivatives in infected humanized mice. (a) Full-length vRNA in the plasma of mice infected with SIVcpz*Ptt* MB897 ($n = 3$), SIVcpz*Ptt* EK505 ($n = 2$), and SIVcpz*Ptt* MT145 ($n = 2$) at 15 wpi was sequenced. Briefly, vRNA was isolated from the plasma of infected mice at 15 wpi, and cDNA was generated. Then, the 11 DNA fragments represented in the figure (fragments A to K) were obtained by RT-PCR using the primers listed in Table 2. Mouse identification numbers are shown on the left of each sequence and are identical to those in Table 1. The mutation g7032a (gp120 G413R) is indicated by a red asterisk. (B) Activity of SIVcpz*Ptt* Vif to counteract human APOBEC3 proteins. The expression plasmids for SIVcpz*Ptt* Vif or HIV-1M NL4-3 Vif (as a positive control) were cotransfected with pNL4-3Δ*vif* and either APOBEC3F or APOBEC3G expression plasmids into HEK293T cells. (Top) TZM-bl cell assay. The infectivity of released virus was determined using TZM-bl cells. The assay was performed in triplicate. The data represent averages with SDs. (Bottom) Western blot. The input of cell lysate was standardized to α-tubulin (TUBA), and representative results are shown. (C) Structural homology model of SIVcpz*Ptt* MB897 gp120 and its G413R derivative. The structure model of gp120 of SIVcpz*Ptt* MB897 (top) and its point mutant, MB897 gp120 G413R (bottom), were generated by homology modeling via the SWISS-Model Server Program based on the crystal structure of the gp120 of HIV-1 clade C strain ZM176.66 (PDB accession number 4JST) as a template. The surface model (left) and cartoon model (middle) of parental MB897 gp120 and its G413R mutant are shown. The residue at position 413 is indicted in red (G413, top) or blue (R413, bottom). The boxed regions in the middle panels are enlarged in the right panels. (D) TZM-bl cell assay. One microgram of the IMCs of SIVcpz*Ptt* MB897 (parental MB897) and its derivative (MB897 gp120 G413R) was individually transfected into HEK293T cells. Forty-eight hours posttransfection, the culture supernatant was harvested as virus preparation (for more detail, see Materials and Methods). The amount of viral particles was quantified by p24 ELISA, and the infectivity of each virus was determined with a TZM-bl cell assay. This assay was performed in triplicate, and averages with SDs are shown. *, $P < 0.05$ by Student's *t* test.

replication capacity in human cells, we prepared two more derivatives of SIVcpz*Ptt* MB897 in addition to the gp120 G413R mutant (Fig. 5A). The M30R substitution in viral MA has been reported to augment the replication kinetics of SIVcpz*Ptt* in *ex vivo* human tonsil histoculture (32). In addition, SIVcpz*Ptt* Vpu is incapable of counteracting human-tetherin-mediated antiviral action (24, 25). Consistently with previous findings (25, 29), we confirmed that SIVcpz*Ptt* Vpu downregulates human CD4 but not human tetherin but that HIV-1M Vpu potently downregulates both of these proteins (Fig. 5B and C). We have previously demonstrated that HIV-1M Vpu augments viral dissemination in our humanized-mouse model (39, 47). To directly evaluate the effect of the antitetherin ability of Vpu on viral propagation *in vivo*, we prepared an SIVcpz*Ptt* MB897 derivative that incorporates the transmembrane domain of HIV-1M (strain NL4-3) Vpu and is designated MB897 NL*vpu*TM, in accordance with a previous report (28). As shown in

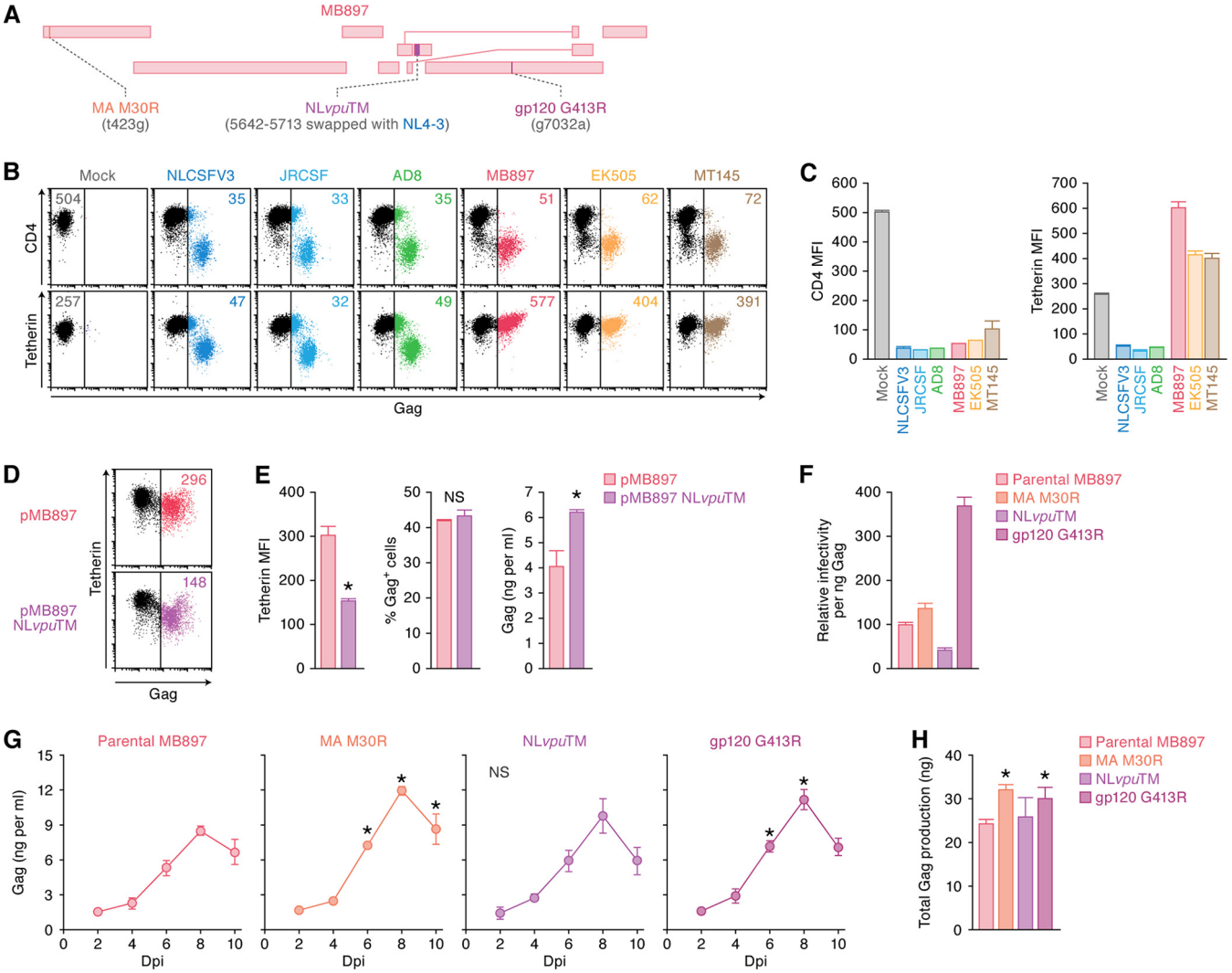

FIG 5 Functional analysis of SIVcpz*Ptt* MB897 derivatives. (A) Scheme of the SIVcpz*Ptt* MB897 derivatives used in this assay. The nucleotide numbers, which are based on the database (accession no. JN835461), are represented in parentheses in gray. (B and C) Activity of SIVcpz*Ptt* Vpu to down-modulate human CD4 and tetherin proteins. Vesicular stomatitis virus Gag (VSVg)-pseudotyped HIV-1M and SIVcpz*Ptt* solutions were inoculated into MT-4 cells at an MOI of 0.1. Forty-eight hours postinfection, the levels of surface CD4 and tetherin on Gag-positive cells were analyzed by flow cytometry. Representative dot plots (B) and a summary of mean fluorescent intensities (MFI) (C) are shown. (D) Activity of MB897 NL*vpu*TM to downregulate human tetherin protein. One microgram of the IMCs of SIVcpz*Ptt* MB897 (pMB897) and MB897 NL*vpu*TM (pMB897 NL*vpu*TM) was individually transfected into HeLa cells. Forty-eight hours posttransfection, the level of surface tetherin on Gag-positive cells and the percentage of Gag-positive cells were analyzed by flow cytometry. Representative dot plots (D) and a summary (E) are shown. The amount of released viral particles in the culture supernatant was quantified by p24 ELISA, and the results are shown in the right portion of panel D. (F) TZM-bl cell assay. One microgram each of the IMCs of SIVcpz*Ptt* MB897 and its derivatives were individually transfected into 293T cells. Forty-eight hours posttransfection, the culture supernatant was harvested as the virus preparation. The amount of viral particles was quantified by p24 ELISA, and the infectivity of each virus was determined using the TZM-bl cell assay. The value of parental MB897 was set to 100 to facilitate comparison. This assay was performed in triplicate, and averages with SDs are shown. (G and H) Viral replication assay in activated human $CD4^+$ T cell culture. (G) PHA-activated human PBMCs were infected with each virus at an MOI of 0.1, and the amount of viral Gag in the culture supernatant was quantified. Dpi, days postinfection; NS, no statistical significance. (H) Cumulative amount of viral Gag. The assay was performed in triplicate, and averages with SDs are shown. (E, G, and H) *, $P < 0.05$ versus the value in parental MB897 (by Student's *t* test).

Fig. 5D and E, the SIVcpz*Ptt* MB897 NL*vpu*TM mutant potently downregulated human tetherin from the surfaces of infected cells. In addition, the amount of released viral particles of this derivative was significantly higher than that of the parental virus (Fig. 5E, right panel), suggesting that the MB897 NL*vpu*TM derivative acquires the ability to antagonize human tetherin.

Using three IMCs of SIVcpz*Ptt* MB897 derivatives, MB897 MA M30R, MB897 NL*vpu*TM, and MB897 gp120 G413R, as well as their parental IMC (Fig. 5A), we prepared virus supernatants by transfecting their plasmids into HEK293T cells and evaluated their infectivities *in vitro*. As shown in Fig. 5F, the TZM-bl cell assay showed that the

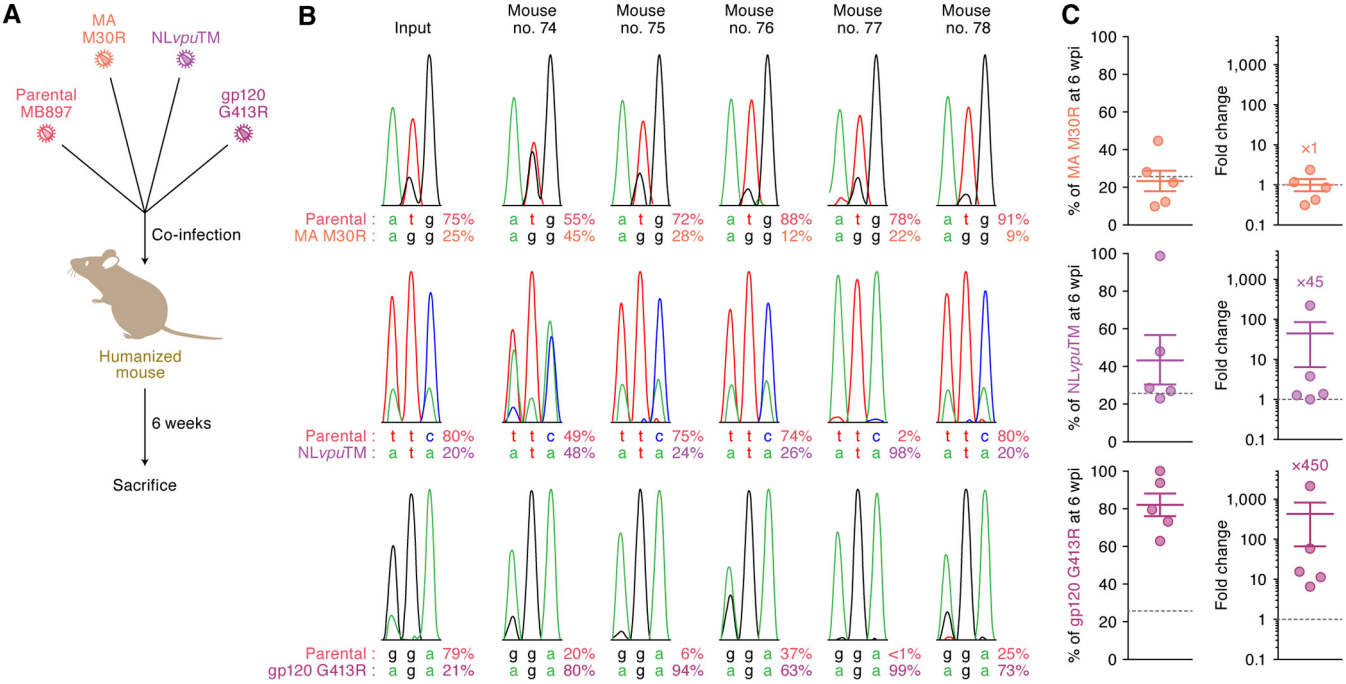

FIG 6 *In vivo* competition assay. (A) Scheme of the *in vivo* competition assay. In this assay, the 4 types of virus preparations containing 1.25 ng of p24 antigen each were coinoculated into humanized mice. After 6 weeks, the infected mice were euthanized and the vRNA in plasma was sequenced. (B and C) Proportion of each virus at 6 wpi. (B) The chromatograms of the sequences of input virus (left) and vRNA in the plasma of 5 infected mice (mouse identification numbers are 74 to 78 and are identical to those in Table 1) at 6 wpi are shown. The chromatograms of the direct sequence of the regions of MA (top), Vpu (middle), and gp120 (bottom) are represented, and the percentage of each sequence is indicated under the chromatogram. (C) The percentage of each mutant at 6 wpi (left) and the fold change of each mutant from the parental virus (right) are shown. The values from each infected mouse are shown by dots. The horizontal bars represent averages with SEMs. In the right panel, the numbers represent the fold change with respect to the parental virus. The values 25% (left) and 1 (right) are indicated by a broken horizontal line.

infectivities of the MA M30R and gp120 G413R strains were 1.4-fold and 3.7-fold higher than that of the parental strain, MB897, respectively, but that the infectivity of MB897 NL*vpu*TM was 0.42-fold lower. By using these viral supernatants and PHA-activated human PBMCs, we performed *in vitro* viral replication assays. Although the viral growth of MB897 NL*vpu*TM was similar to that of parental MB897, the MA M30R and gp120 G413R derivatives replicated more efficiently than the parental virus, with statistical significance (Fig. 5G). Also, the cumulative amount of viral Gag in the culture supernatants of the MA M30R and gp120 G413R strains was significantly higher than that of the parental virus (Fig. 5H), suggesting that these two mutations positively contribute to viral fitness in the culture of PHA-activated human PBMCs *in vitro*.

To elucidate the replication kinetics of these viruses *in vivo*, equal amounts of each virus supernatant were used to inoculate five humanized mice in an *in vivo* competition assay (Fig. 6A) (37). After 6 weeks, the five infected mice were euthanized and the sequence of vRNA in the plasma was directly analyzed. As shown in Fig. 6B and C, the replication capacity of the MA M30R derivative was comparable to that of the parental virus, which suggests that the MA M30R mutation is not advantageous for viral replication *in vivo*. In contrast, the proportions of the MB897 NL*vpu*TM and gp120 G413R derivatives were higher than that of the parental virus, which implies more-efficient replication (Fig. 6B and C). Taken together, these findings suggest that the acquisition of activity to antagonize tetherin (i.e., the mutation in *vpu*) and the augmentation of viral infectivity (e.g., for gp120 G413R) are important for SIVcpz to fully adapt to infect humans.

To further investigate the effect of adaptive mutations on the replication efficacy of SIVcpz *in vivo*, we prepared an SIVcpz*Ptt* MB897 derivative that possesses all three mutations, MA M30R, NL*vpu*TM, and gp120 G413R, and designated it MB897 3mut. We inoculated this virus into eight humanized mice at the same amount as parental MB897,

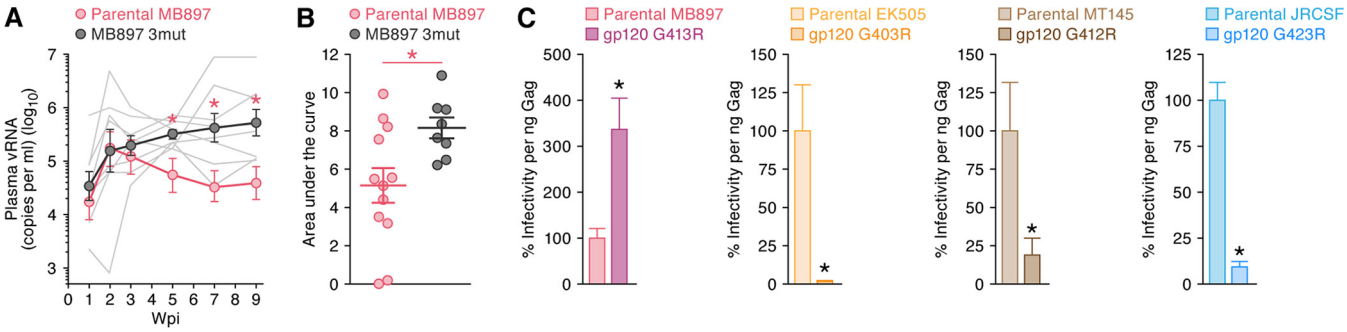

FIG 7 Investigation of the adaptive mutation of SIVcpz in humanized mice. (A and B) The virus supernatants containing 5 ng of p24 antigen (SIVcpz*Ptt* parental MB897 [$n = 10$] or MB897 3mut derivative [$n = 8$]) were inoculated into humanized mice, and the amounts of vRNA in the plasma (A) were analyzed at 0, 1, 2, 3, 5, 7, and 9 wpi. Each average with SEM is shown as a dot with an error bar, and the values from each mouse are shown by lines. *x* axes, numbers of weeks postinfection. (A) The detection limit of HIV-1 RNA is 800 copies/ml plasma, and the results of parental MB897 are identical to those in Fig. 2A. (B) Area under the curve of the plasma vRNA. (C) TZM-bl cell assay. One microgram of each IMC was individually transfected into HEK293T cells. Forty-eight hours posttransfection, the culture supernatant was harvested as the virus preparation. The amount of viral particles was quantified by p24 ELISA, and the infectivity of each virus was determined using the TZM-bl cell assay. The value of parental virus was set to 100 to facilitate comparison. This assay was performed in triplicate, and averages with SDs are shown. (A and B) Asterisks indicate statistically significant differences ($P < 0.05$ by the Mann-Whitney U test) from parental MB897. (C) Asterisks indicate statistically significant differences ($P < 0.05$ by Student's *t* test) from the respective parental virus.

and the plasma vRNA was longitudinally monitored until 9 wpi. As shown in Fig. 7A, we found that the plasma vRNA of MB897 3mut was significantly higher than that of parental MB897 after 5 wpi. We confirmed that no reversion occurred in all eight infected mice. Moreover, the area under the curve of the plasma vRNA of the MB897 3mut derivative was significantly higher than that of parental MB897 (Fig. 7B). These findings suggest that these three mutations beneficially contribute to the efficacy of viral replication *in vivo*.

Finally, we evaluated the effect of the G-to-R mutation in gp120 on different virus strains. Because this glycine is highly conserved in HIV-1/SIVcpz in the C4 region of gp120, we changed this glycine of SIVcpz*Ptt* strains EK505 (G403R) and MT145 (G412R) and HIV-1 strain JR-CSF (G423R) to arginine. As shown in Fig. 7C, although this mutation significantly increased the infectivity of MB897, the infectivity of the other viruses was significantly decreased by this G-to-R mutation. Taken together, these findings suggest that the G-to-R mutation in the C4 region of gp120 is beneficial only for SIVcpz*Ptt* MB897.

DISCUSSION

In this study, we inoculated three strains of SIVcpz*Ptt*, MB897, EK505, and MT145, into humanized mice and investigated the replication kinetics and pathogenicity of SIVcpz*Ptt* *in vivo* in comparison with those of HIV-1M and HIV-1N. Chimpanzees that were naturally or artificially infected with SIVcpz have been used to assess viral pathogenesis (48, 49). Indeed, one study previously suggested that wild chimpanzees that are naturally infected with SIVcpz exhibit AIDS-like immunopathology and higher rates of mortality than uninfected chimpanzees (50). However, as the use of chimpanzees for invasive experiments is now strictly and ethically prohibited, it is technically difficult to conduct experiments that characterize the pathogenic effects of SIVcpz infection *in vivo*. Moreover, because of viral diversity (i.e., SIVcpz*Ptt* and SIVcpz*Pts*, where "*Pts*" indicates *Pan troglodytes schweinfurthii*) (12, 51, 52) and the hosts of these viruses (i.e., chimpanzee subspecies, such as *Pan troglodytes troglodytes* and *Pan troglodytes schweinfurthii*) (53), the outcome of SIVcpz infection in animals remains unknown. Using our humanized-mouse model, we demonstrate that SIVcpz*Ptt* efficiently replicates in humanized mice (Fig. 2A). Moreover, we show that viral pathogenicity (i.e., the decrease of peripheral $CD4^+$ T cells) significantly correlates with the level of acute viremia. Lastly, infection with SIVcpz*Ptt* MB897 yields a phenotype that is more similar, in terms of acute viremia and pathogenicity, to that of HIV-1M than to that of the other SIVcpz*Ptt* (e.g., EK505 and MT145) and HIV-1N (Fig. 3) strains. As SIVcpz*Ptt*

MB897 is the phylogenetically closest SIVcpz*Ptt* relative of HIV-M (Fig. 1A) (12), our findings suggest that pandemic HIV-1 (i.e., HIV-1M) has emerged partly due to the preadaptation of certain SIVcpz*Ptt* strains, such as MB897.

Consistently with the previously proposed model (12–15), our findings support a hypothesis that the exposure of certain MB897-related SIVcpz*Ptt* viruses, as opposed to other SIVcpz*Ptt* strains, to humans in Central Africa resulted in the emergence of pandemic HIV-1 following initial preadaptation. Intriguingly, based on the *in vitro* culture of primary human $CD4^+$ T cells, the infectivity (Fig. 1C) and replication kinetics of SIVcpz*Ptt* MB897 (54) were similar to, or even lower than, those of the other SIVcpz*Ptt* strains and HIV-1 strains assessed. Therefore, this is the first report to demonstrate that SIVcpz*Ptt* MB897 has a virological phenotype similar to that of pandemic HIV-1.

To our knowledge, this is the first study to use HIV-1N, another HIV-1 group originating from the cross-species transmission of SIVcpz*Ptt* (12, 55, 56), in addition to SIVcpz*Ptt*, in a humanized-mouse model of infection. As only a dozen patients infected with HIV-1N have been reported in Cameroon (18, 19), the pathogenicity and replication kinetics of HIV-1N *in vivo* have not been fully elucidated. Using our humanized-mouse model, we demonstrate that two strains of HIV-1N, DJO1031 and YBF30, undergo *in vivo* replication with kinetics (Fig. 2A) and associated pathogenic effects (Fig. 2B) that are significantly lower than those of HIV-1M infection. Furthermore, the acute viremia (Fig. 2F) in the PB of HIV-1N-infected humanized mice (Fig. 2F) was lower than that of SIVcpz*Ptt* MB897-infected mice. In this regard, previous molecular virology studies have shown that the Vpu proteins of HIV-1N and SIVcpz*Ptt* EK505, which are phylogenetically related viruses (Fig. 1A), are less efficient at degrading CD4 molecules than the Vpu proteins of HIV-1M and SIVcpz*Ptt* MB897 (29, 57), although HIV-1N Nef is functionally comparable to those of HIV-1M and SIVcpz*Ptt* MB897 (58). Additionally, most of the Vpu proteins encoded by HIV-1N strains, including DJO1031 and YBF30, are incapable of antagonizing human tetherin, which is a restriction factor for HIV-1 replication (29, 57). In fact, we have previously demonstrated that HIV-1M Vpu antagonizes human tetherin and thereby promotes efficient viral replication in humanized mice (39). Therefore, the reason for a significantly lower viral load in HIV-1N-infected humanized mice than in mice infected with HIV-1M (Fig. 2A) may be partly the lack of anti-tetherin activity. Furthermore, previous molecular phylogenetic studies have estimated that HIV-1N originated in the 1960s (16) and is younger than HIV-1M, which is estimated to have emerged in the 1920s (17). Taken together with these previous reports, our findings further suggest that HIV-1N is not yet optimally adapted to infect humans.

As only Vpu of HIV-1M commonly confers the ability to counteract human tetherin (29), the acquisition of the ability to antagonize human tetherin by HIV-1M Vpu may have contributed to the worldwide HIV-1M pandemic (25). In fact, through an experimental-mathematical approach, we have recently reported that human tetherin works as a factor of intrinsic herd immunity against HIV-1 but that HIV-1M Vpu overcomes human tetherin-mediated herd immunity and enhances the efficiency of human-to-human transmission (31). Moreover, Sauter et al. (57) revealed that the Vpu protein of an HIV-1N strain N1Fr2011, which has recently been introduced into Europe from Cameroon (59), has the ability to antagonize human tetherin. This observation further suggests the importance of Vpu-mediated human tetherin antagonism in viral spread throughout the human population. Furthermore, as described above, we have previously demonstrated that Vpu of HIV-1M promotes viral replication in humanized mice via loss-of-function experiments (39). Additionally, for this study, we performed gain-of-function experiments using SIVcpz*Ptt* MB897 NL*vpu*TM, a mutant of MB897 that incorporates the Vpu transmembrane region of HIV-1M, to demonstrate that the ability to antagonize human tetherin promotes the efficiency of viral replication in humanized mice (Fig. 6). Our findings strongly suggest that harnessing an antagonistic ability against human tetherin by Vpu is a crucial step for SIVcpz*Ptt* to fully adapt to infect humans.

Through analyzing the full-length sequences of vRNA in mice infected with SIVcpz*Ptt*,

we detected a common mutation, gp120 G413R, in SIVcpz*Ptt* MB897-infected mice (Fig. 4A). This mutant was already detected in a previous study by Yuan et al. (33), but the virological effect of this mutation has not been addressed. Interestingly, we herein demonstrate that this mutation increases viral infectivity *in vitro* (Fig. 4B) and replication efficacy in humanized mice (Fig. 6). Our results suggest that gp120 G413R is a favorable mutation for SIVcpz*Ptt* MB897 to infect humans by augmenting viral infectivity. To the best of our knowledge, this is the first study to demonstrate an adaptive mutation of SIVcpz*Ptt* to infect humans *in vivo* and further implies that the augmentation of viral infectivity is a crucial step for modulating the viral fitness of SIVcpz*Ptt* in humans. Moreover, as this nonsynonymous mutation that we found is in gp120, it is assumed that the gp120 G413R mutation may improve the ability of SIVcpz*Ptt* MB897 to use human CD4 and/or CCR5 as opposed to chimpanzee receptors and further promote viral adaptation to humans. This issue is intriguing and will be addressed in a future investigation.

Regarding adaptive mutations of SIVcpz*Ptt*, the M30K/R substitution in Gag MA is considered a species-specific adaptive change based on the following three observations: (i) arginine (R) or lysine (K) at position 30 of MA is a highly conserved residue in HIV-1, while all SIVcpz*Ptt* viruses detected thus far encode methionine at this position (43); (ii) chimpanzee-adapted HIV-1 viruses, strains JC16 and NC7 (60), encode methionine (M) at position 30 of MA (43); and (iii) the M30K/R mutation facilitates SIVcpz*Ptt* replication in human tonsil histoculture *ex vivo* (32). However, how the amino acid at position 30 of MA contributes to species-specific adaptation remains unclear. In accordance with these previous studies, we used an MA M30R derivative of SIVcpz*Ptt* MB897 to assess differences in replication efficiency. Although the viral growth of the MA M30R derivative was significantly higher than that of parental MB897 in *in vitro* culture of activated human $CD4^+$ T cells (Fig. 5G and H), the replication kinetics of this derivative in humanized mice was comparable to that of parental virus (Fig. 6). Taken together with those of previous studies (32, 43, 60), our findings imply that the impact of the amino acid at position 30 of MA may depend on the experimental systems used. In fact, this M30K/R mutant did not emerge *de novo* in our humanized mice infected with SIVcpz*Ptt* (Fig. 4A), and a previous study using a BLT–humanized-mouse model (33). To elucidate the functional effect of the M30K/R substitution in Gag MA on viral fitness, further investigations using various experimental systems will be needed. The evolutionary scenario of the emergence of HIV-1 from SIVcpz might be a more complicated event than expected, and therefore, multiple experimental approaches are crucial to address this issue. Although we did not observe a clear difference on the M30R derivative in infected humanized mice, here we provided conclusive evidence that gp120 M143R and *vpu* mutants positively contribute to viral fitness *in vivo* (Fig. 6).

Although the acute vRNA level of SIVcpz*Ptt* MB897-infected mice was comparable to that of HIV-1M-infected mice and was significantly higher than those of the mice infected with HIV-1N and the other SIVcpz*Ptt* strains (Fig. 2A and B), the chronic vRNA level of SIVcpz*Ptt* MB897-infected mice was significantly lower than that of HIV-1M-infected mice (Fig. 2A). Also, the levels of chronic vRNA of the mice infected with HIV-1N, SIVcpz*Ptt* EK505, and SIVcpz*Ptt* MT145 were significantly lower than that of mice infected with HIV-1M (Fig. 2A). These observations suggest that HIV-1M is more optimally adapted to infect humans than the other viruses. Importantly, only HIV-1M Vpu potently antagonizes the antiviral action of human tetherin (29), and our experimental-mathematical analyses have recently shown that HIV-1M Vpu markedly increases the rate of viral replication *in vivo* (47). All together, these findings strongly suggest that the Vpu-tetherin interaction may be a critical step for increasing viral fitness *in vivo*. On the other hand, consistently with previous reports (45, 61), human APOBEC3F and APOBEC3G, which represent another type of antiviral restriction factor, were efficiently counteracted by the action of SIVcpz*Ptt* Vif (Fig. 4B), suggesting that the Vif-APOBEC3 interaction is not a human-specific hurdle, at least for SIVcpz*Ptt*. Our findings raise the possibility of a not-yet-identified factor(s) that maintains a high vRNA level *in vivo* during the chronic phase of infection and that can be antagonized only by HIV-1M. In this regard, we directly demonstrated that the chronic vRNA level of the

MB897 3mut derivative was significantly higher than that of parental MB897 (Fig. 7A). Taken together, this is the first report directly demonstrating the adaptation of SIVcpz to humans *in vivo*.

A study conducting SIVcpz infection using a BLT–humanized-mouse model was reported by Yuan et al. during the preparation of this paper (33). Compared to this paper (33), however, our study reports at least three major updates. First, we tested the viral fitness of two HIV-1 groups, M and N, both of which originated from the cross-species transmission of SIVcpz*Ptt* (12). Although the virological characteristics of nonpandemic HIV-1N strains are of interest in considering the evolutionary scenario of HIV-1/SIVcpz, only a few studies have been conducted, and little is known about this issue. To our knowledge, this is the first study recapitulating the viral pathogenesis of HIV-1N in an *in vivo* model and providing insights into virological characteristics of HIV-1N. Second, through statistical analyses of various virological parameters, we showed that there is a statistically significant correlation between the viral load during the acute phase of infection and the level of $CD4^+$ T-cell decrease in PB (Fig. 3). Based on these findings, we provide evidence suggesting that SIVcpz*Ptt* strain MB897, which is the strain phylogenetically closest to pandemic HIV-1, potently exhibits virological characteristics similar to those of pandemic HIV-1. Third, we detected a *de novo* mutation in the *env* gene of MB897-infected mice (Fig. 4A). Although this mutation was already identified by Yuan et al. (33), its effect on viral infection and replication had not been addressed. For this study, we prepared an IMC of strain MB897 harboring this mutation and revealed that the gp120 M413R mutation significantly increases viral infectivity *in vitro* (Fig. 4D and 5G and H) and *in vivo* (Fig. 6). These findings are novel and strongly suggest that the gp120 M143R mutation is beneficial for SIVcpz*Ptt* strain MB897 to augment viral infectivity and presumably to promote viral adaptation to humans.

MATERIALS AND METHODS

Ethics statement. All procedures, including animal experiments, were conducted by following the guidelines for the care and use of laboratory animals of the Ministry of Education, Culture, Sports, Science, and Technology of Japan (62). The authors received approval from the Institutional Animal Care and Use Committees (IACUC)/ethics committee of the institutional review board of Kyoto University (protocol number D13-25). All protocols involving human subjects were reviewed and approved by the Kyoto University institutional review board. All human subjects provided written informed consent from adults.

Humanized mice. NOG mice (NOD SCID *Il2r* knockout mice) (63) were obtained from the Central Institute for Experimental Animals (Kawasaki, Kanagawa, Japan). The mice were maintained under specific-pathogen-free conditions and were handled in accordance with the regulation of the IACUC/ethics committee of Kyoto University. Human $CD34^+$ hematopoietic stem cells were isolated from human fetal liver as previously described (64). The humanized-mouse model (with NOG-hCD34 mice) was constructed as previously described (34–36, 38, 39, 65). Briefly, 86 newborn (aged 0 to 2 days) NOG mice from 29 litters were irradiated with X rays (10 cGy per mouse) using an RX-650 X-ray cabinet system (Faxitron X-ray Corporation) and were then intrahepatically injected with the obtained human-fetal-liver-derived $CD34^+$ cells (7.3×10^4 to 40.0×10^4 cells). A list of the humanized mice used in this study is provided in Table 1.

Cell culture. HEK293T cells (a human embryonic kidney 293 T cell line; ATCC CRL-1573) and TZM-bl cells (obtained through the NIH AIDS Research and Reference Reagent Program) (66) were maintained in Dulbecco's modified Eagle's medium (Sigma) containing fetal calf serum (FCS) and antibiotics. MT-4 cells (a human T cell leukemia cell line) and PHA-activated human PBMCs were maintained in RPMI 1640 (Sigma) containing FCS and antibiotics. Human PBMCs were activated with PHA (Sigma; 1 μg/ml) and maintained with human interleukin-2 (100 U/ml) as previously described (39, 67).

Molecular phylogenetics. The 17 concatenated HIV-1/SIVcpz protein sequences (Gag, Pol, Vif, Vpr, Tat, Rev, Vpu, Env, and Nef) were aligned using Clustal W implemented in MEGA5 (68). Then, the phylogenetic tree was reconstructed using the maximum-likelihood method with the LG+G model using PhyML3.1 (69).

Plasmid construction. To construct pMB897 gp120 G413R, overlap extension PCR was performed using PrimeSTAR GXL DNA polymerase (TaKaRa) according to the manufacturer's protocol, pMB897 as the template, and the following primers: MB897-I-F1, MB897-I-R1 (Table 2), pMB897 7017-7050 fwd (5′-CAG TGG CAA GGA GTA AGA AAA GGA ATC TTT GCA C-3′), and pMB897 7017-7050 rev (5′-GTG CAA AGA TTC CTT TTC TTA CTC CTT GCC ACT G-3′). The resulting DNA fragment was digested with NheI and StuI and then subcloned into the NheI-StuI site of pMB897. To construct pMB897 NL*vpu*TM, overlap extension PCR was performed using PrimeSTAR GXL DNA polymerase according to the manufacturer's protocol, with pMB897 as the template, and the following primers: CON-F-F1, MB897-H-R1 (Table 2),

TABLE 1 Humanized mice used in this study

Mouse	Recipient mouse		Transplanted hHSCs[c]		Inoculated virus	Inoculated age (no. of wks)
	Lot[a]	Sex[b]	Donor lot[d]	No. of cells		
1	74	M	A	73,000	Mock	14
2	75	F	A	73,000	Mock	14
3	76	F	A	73,000	Mock	14
4	96	F	B	120,000	Mock	14
5	96	M	B	120,000	Mock	14
6	165	F	C	170,000	MB897	14
7	165	M	C	170,000	JRCSF	14
8	165	M	C	170,000	MB897	14
9	168	F	C	130,000	AD8	15
10	168	F	C	130,000	AD8	15
11	168	F	C	130,000	MB897	15
12	168	M	C	130,000	MB897	15
13	168	M	C	130,000	EK505	15
14	168	M	C	130,000	Mock	15
15	169	F	C	135,000	Mock	13
16	169	F	C	135,000	MB897	13
17	169	M	C	135,000	EK505	13
18	169	M	C	135,000	EK505	13
19	169	M	C	135,000	MT145	13
20	169	M	C	135,000	MT145	13
21	171	M	D	80,000	Mock	15
22	171	M	D	80,000	Mock	15
23	173	F	C	80,000	MB897	15
24	173	F	C	80,000	Mock	15
25	173	F	C	80,000	AD8	15
26	173	M	C	80,000	MB897	15
27	177	M	D	100,000	Mock	15
28	179	M	E	400,000	JRCSF	17
29	180	F	D	200,000	Mock	11
30	180	F	D	200,000	Mock	11
31	181	F	F	180,000	EK505	10
32	181	F	F	180,000	EK505	10
33	181	F	F	180,000	EK505	10
34	181	F	F	180,000	MT145	10
35	181	M	F	180,000	MT145	10
36	191	F	G	230,000	JRCSF	19
37	191	F	G	230,000	JRCSF	19
38	191	M	G	230,000	AD8	19
39	191	M	G	230,000	JRCSF	19
40	192	M	F	260,000	AD8	17
41	192	M	F	260,000	AD8	17
42	194	F	E	100,000	MB897	15
43	194	F	E	100,000	MB897	15
44	194	F	E	100,000	MB897	15
45	194	M	E	100,000	DJO0131	15
46	194	M	E	100,000	DJO0131	15
47	195	F	F	120,000	EK505	17
48	195	M	F	120,000	MT145	17
49	195	M	F	120,000	MT145	17
50	195	M	F	120,000	MT145	17
51	196	F	F	120,000	EK505	16
52	196	F	F	120,000	DJO0131	16
53	196	F	F	120,000	DJO0131	16
54	196	M	F	120,000	DJO0131	16
55	196	M	F	120,000	DJO0131	16
56	197	F	G	100,000	EK505	16
57	197	M	G	100,000	Mock	16
58	197	M	G	100,000	DJO0131	16

(Continued on next page)

TABLE 1 (Continued)

Mouse	Recipient mouse		Transplanted hHSCs[c]		Inoculated virus	Inoculated age (no. of wks)
	Lot[a]	Sex[b]	Donor lot[d]	No. of cells		
59	197	M	G	100,000	DJO0131	16
60	198	M	G	100,000	MB897	16
61	198	M	G	100,000	MT145	16
62	198	M	G	100,000	MT145	16
63	198	M	G	100,000	DJO0131	16
64	198	M	G	100,000	DJO0131	16
65	198	M	G	100,000	MB897	16
66	208	F	H	100,000	DJO0131	15
67	208	M	H	100,000	YBF30	15
68	208	M	H	100,000	YBF30	15
69	208	M	H	100,000	YBF30	15
70	209	F	I	100,000	YBF30	14
71	209	F	I	100,000	YBF30	14
72	209	F	I	100,000	YBF30	14
73	209	M	J	100,000	DJO0131	14
74	214	M	K	196,000	MB897 derivatives	18
75	214	M	K	196,000	MB897 derivatives	18
76	215	F	L	100,000	MB897 derivatives	15
77	215	F	L	100,000	MB897 derivatives	15
78	215	M	L	100,000	MB897 derivatives	15
79	274	M	M	100,000	MB897 3mut	21
80	278	F	N	130,000	MB897 3mut	15
81	279	F	O	113,000	MB897 3mut	15
82	281	F	P	110,000	MB897 3mut	14
83	283	M	Q	250,000	MB897 3mut	14
84	283	M	Q	250,000	MB897 3mut	14
85	283	M	Q	250,000	MB897 3mut	14
86	283	M	Q	250,000	MB897 3mut	14

[a]Twenty-nine lots of newborn NOG mice were used as the recipient.
[b]F, female; M, male.
[c]hHSCs, human $CD34^+$ hematopoietic stem cells.
[d]NOG– human-CD34 mice were reconstructed with one of 17 donors.

MB897 NL*vpu*TM fwd (5′-ATT AGT AGT AGC AAT AAT AAT AGC AAT AGT TGT GTG GTC CAT AGT AAT CAT ATG TTA TAA GGC ACT TAA AAG AC-3′), and MB897 NL*vpu*TM rev (5′-TTG CTA TTA TTA TTG CTA CTA CTA ATG CTA CTA TTG CTA CTA TTA TTA TTT CCA TAT ATT ATA TTA CAC TTA TT-3′). The resulting DNA fragment was digested with HpaI and AclI and then subcloned into the HpaI-AclI site of pMB897. The sequences of these constructed plasmids were confirmed by Sanger sequencing. pMB897 matrix (MA) M30R was kindly provided by Frank Kirchhoff (Ulm University, Ulm, Germany) (32).

Virus preparation and infection. The following viruses were used in this study: 4 strains of HIV-1M, namely, NL4-3 (70), NLCSFV3 (71), JRCSF (72), and AD8 (73); 2 strains of HIV-1N, namely, YBF30 (obtained from the NIH reagent program) and DJO0131 (kindly provided by Frank Kirchhoff and Beatrice H. Hahn) (57); and 3 strains of SIVcpz*Ptt*, namely, MB897, EK505, and MT145 (kindly provided by Beatrice H. Hahn). The accession numbers and brief characteristics of these viruses are summarized in Fig. 1B. To prepare virus supernatants for the experiments using humanized mice, 30 μg of IMCs was transfected into HEK293T cells according to the calcium phosphate method as previously described (38–41). At 48 h posttransfection, the culture supernatant was harvested, centrifuged, and then filtered through a 0.45-μm filter (Millipore) to obtain the virus supernatant. The amount of viral particles (Gag) was quantified using an HIV-1 p24 antigen enzyme-linked immunosorbent assay (ELISA) kit (Zeptometrix). Virus supernatants containing 5 ng (Fig. 2 and 7A) or 1.25 ng (Fig. 6) of Gag antigen were intraperitoneally inoculated into NOG-hCD34 mice. RPMI 1640 was used for mock infection. For the viral replication assay in *in vitro* cell cultures, PHA-activated human PBMCs were prepared as described above. These cells were infected with each virus at a multiplicity of infection (MOI) of 0.1, and the culture supernatant was harvested every 2 days as previously described (39, 67). The amount of viral particles in the culture supernatant was quantified using an HIV-1 p24 ELISA kit (Zeptometrix) as described above.

PB collection, mononuclear cell isolation, and quantification of HIV-1 vRNA in plasma. PB and plasma were routinely collected as previously described (34, 38–41). The mice were euthanized at 15 weeks postinfection (wpi) (Fig. 2) with anesthesia, and the spleen was crushed, rubbed, and suspended as previously described (34, 38–41). To obtain splenic human mononuclear cells, the splenic cell suspension was separated using Ficoll-Paque (Pharmacia) as previously described (34, 38–41). The

TABLE 2 Primers used for the sequencing of full-length viruses

Virus strain	Fragment	Primer name	Sequence of forward primer (5′ to 3′)	Primer name	Sequence of reverse primer (5′ to 3′)	Amplicon length (bp)
MB897	A	CON-A-F1	ACTGGGTCTCTCTKGTTAGACC	MB897-A-R1	CTTTTACTCTAATTCTTTGATG	553
		MB897-A-F2	GTCTCTCTKGTTAGACCAGATT	MB897-A-R2	TTCTGATCCTGTTGTGAGAGCTGG	
	B	CON-B-F1	ATGGGTGCGAGAGCGTC	CON-B-R1	TCYTTKCCACAATTRAARCA	1,115
		CON-B-F2	ATGAAACATTTAGTATGGGCAAG	MB897-B-R2	GCTTCWGCTARNACYCTWGCCTTATG	
	C	MB897-C-F1	AGAGTGGGACAGGACACACC	CON-C-R1	CTTCATCTAGGGGGCATGAA	1,430
		MB897-C-F2	GCAGGGACAACTAGCACCAT	MB897-C-R2	TCCTAGCTGGACTTCCCAAA	
	D	MB897-D-F1	GGGAATTGGAGGTTTTATAAAAGTAAGAC	MB897-D-R1	CAGATGACTATACTTTCCAGGGCTACT	1,062
		MB897-D-F2	AAAGAGCAATAGGTACAGTATTAGTAGGGC	MB897-D-R2	TAACTCTAATTCTGCTTCCTGTGTGAG	
	E	MB897-E-F1	TCCAGCTAGGAATACCACACCC	MB897-E-R1	TGAATGATCCCTAATGCATATTGTG	1,118
		MB897-E-F2	CCAGTACATGGATGATCTATATGTAGGATC	MB897-E-R2	TCCCTCTATCAGTTACATATCCTGCTTT	
	F	CON-F-F1	TGGTGGDCWGANTAYTGGCA	CON-F-R1	ACBACYGCNCCTTCHCCTTTC	1,009
		CON-F-F2	ACCTGGATHCCHGANTGGGA	CON-F-R2	CCAATYCCYCCYYTTYKYTTAAAATT	
	G	MB897-G-F1	GAATTTGGAATTCCCTACAATCC	MB897-G-R1	AGTTTTAGGCTGACTTCCTGGATG	1,213
		MB897-G-F2	CAATGAACAAAGAGTTAAAGAAAAT	MB897-G-R2	TCTARRYTAGGATCTAYTGGCTCCAT	
	H	MB897-H-F1	GCTATMATAAGAATYCTGCAACAACT	MB897-H-R1	TTTGGACAAGCCTGGGTTATGGCTG	970
		MB897-H-F2	TGYCAWCATAGCAGAATAGGCAT	MB897-H-R2	CTTCTTATCTCTTAATTCTGT	
	I	MB897-I-F1	GCATGGAACAATAACATGGTAGACCAAATG	MB897-I-R1	TTCTGGCCTGTACCGTCAGCGT	1,249
		MB897-I-F2	GGGATCAAAGCCTAAAGCCATGTG	CON-I-R2	GCGCCCATAGTGCTTCCTGCT	
	J	MB897-J-F1	GTGCAGAATAAGACAAATTGTAA	MB897-J-R1	AAGGGGTCTGGAACGACAAAGGTG	818
		MB897-J-F2	TGGCAAAGAGTAGGGAAAGGAAT	CPZ-J-R2	TCCTACTATCATTATGAATATTTTTATATA	
	K	MB897-K-F1	GAAAGAGATTGATAACTACACAGA	CON-K-R1	CACTCAAGGCAAGCTTTAT	1,428
		MB897-K-F2	TGGTCAAGCCTGTGGAATTGGTT	CON-K-R2	AAGGCAAGCTTTATTGAGGC	
EK505	A	CON-A-F1	ACTGGGTCTCTCTKGTTAGACC	EK505-A-R1	AGCTTCCTGTGTATTCTGTACC	553
		EK505-A-F2	GTCTCTCTKGTTAGACCAGATT	EK505-A-R2	CAGTCCTTCTGACCCTGTTTTGAG	
	B	CON-B-F1	ATGGGTGCGAGAGCGTC	EK505-B-R1	TAGATGGCCCTCTTTACCAC	1,121
		EK505-B-F2	ACTTAGTATGGGCAAGCAGGGA	EK505-B-R2	TTGTGCCTGTGTCATGGCTT	
	C	EK505-C-F1	AGAGTGGGACAGGGGACAT	EK505-C-R1	TTCTTCTTTAGCCCTGCTGG	1,438
		EK505-C-F2	CCAAGAGGAAGTGATATAGC	EK505-C-R2	GGGATTCCTAATTGTACTTCC	
	D	CON-D-F1	ATGATAGGGGGAATTGGAGG	EK505-D-R1	CTGCTTCTGGATCTCTGCTA	1,084
		EK505-D-F2	GGGAAAAAAGCAGTTGGCACAG	EK505-D-R2	TCCCTATTCTCAGCTAACTC	
	E	EK505-E-F1	GGGAAGTACAATTAGGAATCCCAC	EK505-E-R1	TTGTCCTGCATCTTGTAAGG	1,151
		EK505-E-F2	CCATTTAGGAAGAACAATCCAG	EK505-E-R2	TTTCTGAGATAGAGGTCACC	
	F	EK505-F-F1	TGGTGGACAGAGTATTGGCA	EK505-F-R1	AACCATCACCTGCCATCTGT	1,260
		EK505-F-F2	ACTTGGATTCCTGATTGGGA	EK505-F-R2	GGACTACTTTTATATCCCCG	
	G	EK505-G-F1	CCTACAATCCTCAAAGTCAGGG	EK505-G-R1	AGGAGTTCTTCGTCGTTGAC	1,321
		EK505-G-F2	GGGTGCAGTAGAATCCATGAA	EK505-G-R2	TTCCTGCCATATGAGATGCC	
	H	EK505-H-F1	GTAGAGGCCATCATTAGGAC	EK505-H-R1	AATGGCAAATCCTGGTGGTG	1,096
		EK505-H-F2	GGCTGTCAACATAGCAGGATAG	EK505-H-R2	TTTTAGGACAGGCCTGTGTC	
	I	EK505-I-F1	TTCAGATGCTAAGGCCCATA	EK505-I-R1	ACACACAGATTTTCCTGAGC	1,463
		EK505-I-F2	GAGGCTCACAATATTTGGGC	EK505-I-R2	AAGTGTTGTTGCGCCTCTAT	
	J	EK505-J-F1	GGACAAGAGTAGGAAAAGGA	EK505-J-R1	TAAGAATCCGCTCACTAAGC	940
		EK505-J-F2	GGAAAAGGAATTTATGCTCCGC	EK505-J-R2	TAGCTCTCCAGCGTCTTCTT	
	K	EK505-K-F1	CATTTTTGGGCTGCTAGAGC	CON-K-R1	CACTCAAGGCAAGCTTTAT	1,489
		EK505-K-F2	GACATTACAAAATGGCTGTGG	CON-K-R2	AAGGCAAGCTTTATTGAGGC	
MT145	A	MT145-A-F1	CAAGGGTCTCTCTTGGTAGACC	MT145-A-R1	ACGGCAGCTTTCAGTTTCTG	655
		MT145-A-F2	GTCTCTCTTGGTAGACCAGATC	MT145-A-R2	CCTGTTGTGTGTCTTCCACT	
	B	CON-B-F1	ATGGGTGCGAGAGCGTC	CON-B-R1	TCYTTKCCACAATTRAARCA	1,124
		CON-B-F2	ATGAAACATTTAGTATGGGCAAG	MT145-B-R2	AGGTCTATTTTGTCCCCCTC	
	C	MT145-C-F1	CAGTGACATAGCAGGCACTA	MT145-C-R1	CTCCATTTGGTGCTGTCCTT	1,204
		MT145-C-F2	CARAATGCNAAYCCAGA	CON-C-R1	CTTCATCTAGGGGGCATGAA	
	D	CON-D-F1	ATGATAGGGGGAATTGGAGG	MT145-D-R1	GGTCATAGTAGGCTCCATGT	1,072
		MT145-D-F2	CCAGTACTGTATTAGTAGGACC	MT145-D-R2	GCCAGTTCTAGTTCAGCTTC	
	E	MT145-E-F1	AGGATGGAAGGGATCTCCTT	MT145-E-R1	GTGGTCTGGGTGTGATTGTA	1,049
		MT145-E-F2	GACTTGTATGTGGGCTCAGA	MT145-E-R2	TATTGGGAGTCAGTGACCAC	
	F	CON-F-F1	TGGTGGDCWGANTAYTGGCA	CON-F-R1	ACBACYGCNCCTTCHCCTTTC	1,054
		CON-F-F2	ACCTGGATHCCHGANTGGGA	CON-F-R2	CCAATYCCYCCYYTTYKYTTAAAATT	
	G	MT145-G-F1	AAGCAGAAGTCATCCCTGCT	MT145-G-R1	TCTAGGTTTGCTCCCTGGAT	1,368
		MT145-G-F2	GGAAGATGGCCAGTAAAGAC	MT145-G-R2	AGTCAGGCTCTATTGGTTCC	
	H	MT145-H-F1	TCTGCCCTCAGTAGCAAAGT	MT145-H-R1	AAATCAGTTGGGTGGTTGCC	1,355
		MT145-H-F2	ACCATCAAGAGAGCCCTATG	MT145-H-R2	AAATCCTGCTGGTGCACAGT	
	I	MT145-I-F1	AAGCTCATAACATCTGGGCC	CON-I-R2	GCGCCCATAGTGCTTCCTGCT	1,332
		MT145-I-F2	CCCAAGCTTGTGTACCTACT	MT145-I-R2	AGAAACAGTGCTCCTAGTCC	
	J	MT145-J-F1	CGAGAAGATCAGGGAGAAGA	MT145-J-R1	ATCCCACTTCTTCATCCTGC	1,352
		MT145-J-F2	CAGGGAGAAGATCAGGATCA	MT145-J-R2	TGTGATACTTCCCCTACTCC	
	K	MT145-K-F1	CCTCTACCACCAATTGAGAG	CON-K-R1	CACTCAAGGCAAGCTTTAT	1,164
		MT145-K-F2	CCTCAGGGGAGTACAACAAA	CON-K-R2	AAGGCAAGCTTTATTGAGGC	

amount of HIV-1 RNA in 50 μl plasma was quantified by Bio Medical Laboratories, Inc. (the detection limit of HIV-1 RNA is 800 copies/ml).

Flow cytometry and hematometry. Flow cytometry was performed with a FACSCanto II instrument (BD Biosciences) as previously described (34, 38–41), and the obtained data were analyzed with Cell

TABLE 3 Accession numbers of HIV-1 and SIVcpz used in Fig. 1A

Virus	Strain	GenBank accession no.
HIV-1M	HXB2	K03455.1
HIV-1M	NL4-3	M19921.2
HIV-1M	JRCSF	M38429.1
HIV-1M	AD8	AF004394.1
SIVcpz*Ptt*	MB897	JN835461.1
HIV-1N	YBF30	AJ006022.1
HIV-1N	DJO0131	AY532635.1
SIVcpz*Ptt*	EK505	JN835460.1
SIVcpz*Ptt*	MT145	JN835462.1
SIVcpz*Ptt*	GAB1	X52154.1
SIVcpz*Ptt*	GAB2	AF382828.1
SIVcpz*Ptt*	CAM3	AF115393.1
SIVcpz*Ptt*	CAM5	AJ271369.1
SIVcpz*Ptt*	CAM13	AY169968.1
SIVcpz*Ptt*	US_Marilyn	AF103818.1
SIVcpz*Pts*	ANT	U42720.2
SIVcpz*Pts*	TAN1	EF394356.1

Quest software (BD Biosciences) and FlowJo software (Tree Star, Inc.). For flow cytometry analysis, anti-CD45–phycoerythrin (PE) (HI30; Biolegend), anti-CD3–allophycocyanin (APC)–Cy7 (HIT3a; Biolegend), anti-CD4–APC (RPA-T4; Biolegend), antitetherin-APC (RS38E; Biolegend), and anti-p24 (Gag)–fluorescein isothiocyanate (FITC) (Kal-1; Dako) antibodies were used. For costaining with intracellular Gag, surface proteins (CD45, CD3, CD4, and tetherin) were stained prior to fixation. Then, the cells were fixed and permeabilized using a Cytofix/Cytoperm solution (BD Biosciences), and intracellular Gag proteins were subsequently stained as previously described (39, 40). Hematometry was performed with a Celltac α MEK6450 analyzer (Nihon Kohden Co.) as previously described (38–41, 65).

Transfection, TZM-bl cell assay, and Western blotting. Transfection, the TZM-bl cell assay, and Western blotting were performed as previously described (38–41). For Western blotting, anti-Flag antibody (M2; Sigma), antihemagglutinin (anti-HA) antibody (3F10; Roche), anti-p24 antiserum (ViroStat), and anti-α-tubulin (TUBA) antibody (DM1A; Sigma) were used.

Sequencing PCR. Sequencing PCR was performed as previously described (41). Briefly, vRNA was extracted from the plasma of infected mice at 15 wpi (Fig. 4A) using a QIAamp viral RNA minikit (Qiagen), and cDNA was prepared as previously described (41). Reverse transcription-PCR (RT-PCR) was performed using PrimeSTAR GXL DNA polymerase according to the manufacturer's protocol, and the primers used are listed in Table 2. The resulting DNA fragments (fragments A to K) (Fig. 4A) were directly sequenced, and the sequence was analyzed with Sequencher v5.1 software (Gene Codes Corporation).

3D homology modeling of SIVcpz*Ptt* MB897 gp120. The three-dimensional (3D) structures of SIVcpz*Ptt* MB897 and its G413R mutant were simulated by the Swiss-Model Server Program (http://swissmodel.expasy.org/) (74–77) based on the crystal structure of HIV-1 clade C strain ZM176.66 gp120 (PDB accession number 4JST) (78) as the template. The generated structure model was refined by energy minimization using the ModRefiner algorithm (79). The structural images were modified and visualized with Pymol 2.0 software.

***In vivo* competition assay.** The *in vivo* competition assay (Fig. 6) was performed as previously described (37). Briefly, four SIVcpz*Ptt* MB897-related viruses (the parental virus MB897, MB897 MA M30R, MB897 NL*vpu*TM, and MB897 gp120 G413R) in preparations containing 1.25 ng of Gag antigen were mixed and were intraperitoneally inoculated into NOG hCD34 mice. At 6 wpi, the infected mice were scarified and vRNA was isolated from the plasma as described above. RT-PCR was performed using PrimeSTAR GXL DNA polymerase according to the manufacturer's protocol and the following primers (listed in Table 2): for the MA region, MB897-A-F2 and MN897-A-R2; for the Vpu region, MB897-H-F2 and MB897-H-R2; and for gp120, MB897-I-F2 and MB897-I-R2. The resulting DNA fragments (Fig. 4A) were directly sequenced, and the sequence was analyzed with Sequencher v5.1 software (Gene Codes Corporation). A similar experiment was performed using the mixed-input virus supernatant and confirmed that each virus was equally present (i.e., at approximately 25% [see the left panel of Fig. 6B]). The percentage of each virus at 6 wpi (Fig. 6C, left panel) was determined using Sequencher v5.1 software according to the procedure previously reported (32). The fold change of each virus at 6 wpi (Fig. 6C, right panel) was calculated as follows: (percentage of the mutant sequence at 6 wpi/percentage of the parental sequence at 6 wpi)/(percentage of the mutant sequence in the input/percentage of the parental sequence in the input).

Statistics. The data are presented as averages $\pm$ standard deviations (SDs) or standard errors of the means (SEMs). Statistically significant differences were determined by Student's *t* test or the Mann-Whitney U test. To determine statistically significant correlations (Fig. 3), the Spearman rank correlation test was applied to the data.

ACKNOWLEDGMENTS

We thank the UCLA Center for AIDS Research (CFAR) Gene and Cellular Therapy Core Facility for providing human CD34$^+$ hematopoietic stem cells. We also thank Ryuichi Kumata and Narumi Saito (Kyoto University, Japan) and Kazuho Higuchi and Tsuzumi Tsukada (Niigata University, Japan) for technical assistance. In addition, we thank Beatrice H. Hahn, Frederic Bibollet-Ruche, and Nicholas F. Parrish (University of Pennsylvania, USA), Frank Kirchhoff and Daniel Sauter (Ulm University Medical Center, Germany), and Dong Sung An (University of California, Los Angeles, CA, USA) for providing materials and crucial suggestions. We appreciate Kotubu Misawa for her dedicated support.

This study was supported in part by grant J-PRIDE 17fm0208006h0001 from the Japan Agency for Medical Research and Development (AMED) (to K.S.), by a grant from CREST, Japan Science and Technology Agency (JST) (to K.S.), by Health Labor Sciences Research grant 26361601 from the Ministry of Health, Labour, and Welfare (MHLW) (to K.S.), by grant-in-aid for scientific research C 15K07166 from the Japan Society for the Promotion of Science (JSPS) (to K.S.), by Scientific Research B (Generative Research Fields) grant 16KT0111 from the JSPS (to K.S.), by Scientific Research on Innovative Areas grants 16H06429, 16K21723, 17H05813 (to K.S.), and 24115008, and by grants from the Ministry of Education, Culture, Sports, Science, and Technology (MEXT) (to Y.K.), the Takeda Science Foundation (to K.S.), the Sumitomo Foundation (to K.S.), the Imai Memorial Trust (to K.S.), the Ichiro Kanehara Foundation (to K.S.), the Kanae Foundation (to K.S.), the Suzuken Memorial Foundation (to K.S.), the Uehara Memorial Foundation (to K.S.), the Mochida Memorial Foundation for Medical and Pharmaceutical Research (to K.S.), the Salt Science Research Foundation (to K.S.), the Smoking Research Foundation (to K.S.), the Chube Ito Foundation (to K.S.), Fordays Self-Reliance Support in Japan (to K.S.), the Mishima Kaiun Memorial Foundation (to K.S.), the Tobe Maki Scholarship Foundation (to K.S.), and the JSPS Core-to-Core Program, A, Advanced Research Networks (to Y.K.). The UCLA CFAR Gene and Cellular Therapy Core Facility is funded through NIH/NIAID grant 5P30 AI028697.

We declare that we have no conflict of interest.

REFERENCES

1. Tong YG, Shi WF, Liu D, Qian J, Liang L, Bo XC, Liu J, Ren HG, Fan H, Ni M, Sun Y, Jin Y, Teng Y, Li Z, Kargbo D, Dafae F, Kanu A, Chen CC, Lan ZH, Jiang H, Luo Y, Lu HJ, Zhang XG, Yang F, Hu Y, Cao YX, Deng YQ, Su HX, Sun Y, Liu WS, Wang Z, Wang CY, Bu ZY, Guo ZD, Zhang LB, Nie WM, Bai CQ, Sun CH, An XP, Xu PS, Zhang XL, Huang Y, Mi ZQ, Yu D, Yao HW, Feng Y, Xia ZP, Zheng XX, Yang ST, Lu B, Jiang JF, Kargbo B, He FC, Gao GF, Cao WC, China Mobile Laboratory Testing Team in Sierra Leone. 2015. Genetic diversity and evolutionary dynamics of Ebola virus in Sierra Leone. Nature 524:93–96. https://doi.org/10.1038/nature14490.
2. Gire SK, Goba A, Andersen KG, Sealfon RS, Park DJ, Kanneh L, Jalloh S, Momoh M, Fullah M, Dudas G, Wohl S, Moses LM, Yozwiak NL, Winnicki S, Matranga CB, Malboeuf CM, Qu J, Gladden AD, Schaffner SF, Yang X, Jiang PP, Nekoui M, Colubri A, Coomber MR, Fonnie M, Moigboi A, Gbakie M, Kamara FK, Tucker V, Konuwa E, Saffa S, Sellu J, Jalloh AA, Kovoma A, Koninga J, Mustapha I, Kargbo K, Foday M, Yillah M, Kanneh F, Robert W, Massally JL, Chapman SB, Bochicchio J, Murphy C, Nusbaum C, Young S, Birren BW, Grant DS, Scheiffelin JS, Lander ES, Happi C, Gevao SM, Gnirke A, Rambaut A, Garry RF, Khan SH, Sabeti PC. 2014. Genomic surveillance elucidates Ebola virus origin and transmission during the 2014 outbreak. Science 345:1369–1372. https://doi.org/10.1126/science.1259657.
3. Carroll MW, Matthews DA, Hiscox JA, Elmore MJ, Pollakis G, Rambaut A, Hewson R, Garcia-Dorival I, Bore JA, Koundouno R, Abdellati S, Afrough B, Aiyepada J, Akhilomen P, Asogun D, Atkinson B, Badusche M, Bah A, Bate S, Baumann J, Becker D, Becker-Ziaja B, Bocquin A, Borremans B, Bosworth A, Boettcher JP, Cannas A, Carletti F, Castilletti C, Clark S, Colavita F, Diederich S, Donatus A, Duraffour S, Ehichioya D, Ellerbrok H, Fernandez-Garcia MD, Fizet A, Fleischmann E, Gryseels S, Hermelink A, Hinzmann J, Hopf-Guevara U, Ighodalo Y, Jameson L, Kelterbaum A, Kis Z, Kloth S, Kohl C, Korva M, et al. 2015. Temporal and spatial analysis of the 2014–2015 Ebola virus outbreak in West Africa. Nature 524:97–101. https://doi.org/10.1038/nature14594.
4. Park DJ, Dudas G, Wohl S, Goba A, Whitmer SL, Andersen KG, Sealfon RS, Ladner JT, Kugelman JR, Matranga CB, Winnicki SM, Qu J, Gire SK, Gladden-Young A, Jalloh S, Nosamiefan D, Yozwiak NL, Moses LM, Jiang PP, Lin AE, Schaffner SF, Bird B, Towner J, Mamoh M, Gbakie M, Kanneh L, Kargbo D, Massally JL, Kamara FK, Konuwa E, Sellu J, Jalloh AA, Mustapha I, Foday M, Yillah M, Erickson BR, Sealy T, Blau D, Paddock C, Brault A, Amman B, Basile J, Bearden S, Belser J, Bergeron E, Campbell S, Chakrabarti A, Dodd K, Flint M, Gibbons A, et al. 2015. Ebola virus epidemiology, transmission, and evolution during seven months in Sierra Leone. Cell 161:1516–1526. https://doi.org/10.1016/j.cell.2015.06.007.
5. Simon-Loriere E, Faye O, Faye O, Koivogui L, Magassouba N, Keita S, Thiberge JM, Diancourt L, Bouchier C, Vandenbogaert M, Caro V, Fall G, Buchmann JP, Matranga CB, Sabeti PC, Manuguerra JC, Holmes EC, Sall AA. 2015. Distinct lineages of Ebola virus in Guinea during the 2014 West African epidemic. Nature 524:102–104. https://doi.org/10.1038/nature14612.
6. Jones KE, Patel NG, Levy MA, Storeygard A, Balk D, Gittleman JL, Daszak P. 2008. Global trends in emerging infectious diseases. Nature 451:990–993. https://doi.org/10.1038/nature06536.
7. Wolfe ND, Dunavan CP, Diamond J. 2007. Origins of major human infectious diseases. Nature 447:279–283. https://doi.org/10.1038/nature05775.
8. Parrish CR, Holmes EC, Morens DM, Park EC, Burke DS, Calisher CH, Laughlin CA, Saif LJ, Daszak P. 2008. Cross-species virus transmission and

the emergence of new epidemic diseases. Microbiol Mol Biol Rev 72:457–470. https://doi.org/10.1128/MMBR.00004-08.
9. Woolhouse ME, Haydon DT, Antia R. 2005. Emerging pathogens: the epidemiology and evolution of species jumps. Trends Ecol Evol 20:238–244. https://doi.org/10.1016/j.tree.2005.02.009.
10. Barre-Sinoussi F, Chermann JC, Rey F, Nugeyre MT, Chamaret S, Gruest J, Dauguet C, Axler-Blin C, Vezinet-Brun F, Rouzioux C, Rozenbaum W, Montagnier L. 1983. Isolation of a T-lymphotropic retrovirus from a patient at risk for acquired immune deficiency syndrome (AIDS). Science 220:868–871. https://doi.org/10.1126/science.6189183.
11. Gallo RC, Sarin PS, Gelmann EP, Robert-Guroff M, Richardson E, Kalyanaraman VS, Mann D, Sidhu GD, Stahl RE, Zolla-Pazner S, Leibowitch J, Popovic M. 1983. Isolation of human T-cell leukemia virus in acquired immune deficiency syndrome (AIDS). Science 220:865–867. https://doi.org/10.1126/science.6601823.
12. Keele BF, Van Heuverswyn F, Li Y, Bailes E, Takehisa J, Santiago ML, Bibollet-Ruche F, Chen Y, Wain LV, Liegeois F, Loul S, Ngole EM, Bienvenue Y, Delaporte E, Brookfield JF, Sharp PM, Shaw GM, Peeters M, Hahn BH. 2006. Chimpanzee reservoirs of pandemic and nonpandemic HIV-1. Science 313:523–526. https://doi.org/10.1126/science.1126531.
13. Faria NR, Rambaut A, Suchard MA, Baele G, Bedford T, Ward MJ, Tatem AJ, Sousa JD, Arinaminpathy N, Pepin J, Posada D, Peeters M, Pybus OG, Lemey P. 2014. HIV epidemiology. The early spread and epidemic ignition of HIV-1 in human populations. Science 346:56–61. https://doi.org/10.1126/science.1256739.
14. de Sousa JD, Alvarez C, Vandamme AM, Muller V. 2012. Enhanced heterosexual transmission hypothesis for the origin of pandemic HIV-1. Viruses 4:1950–1983. https://doi.org/10.3390/v4101950.
15. Sharp PM, Hahn BH. 2008. AIDS: prehistory of HIV-1. Nature 455:605–606. https://doi.org/10.1038/455605a.
16. Wertheim JO, Worobey M. 2009. Dating the age of the SIV lineages that gave rise to HIV-1 and HIV-2. PLoS Comput Biol 5:e1000377. https://doi.org/10.1371/journal.pcbi.1000377.
17. Worobey M, Gemmel M, Teuwen DE, Haselkorn T, Kunstman K, Bunce M, Muyembe JJ, Kabongo JM, Kalengayi RM, Van Marck E, Gilbert MT, Wolinsky SM. 2008. Direct evidence of extensive diversity of HIV-1 in Kinshasa by 1960. Nature 455:661–664. https://doi.org/10.1038/nature07390.
18. Vallari A, Bodelle P, Ngansop C, Makamche F, Ndembi N, Mbanya D, Kaptue L, Gurtler LG, McArthur CP, Devare SG, Brennan CA. 2010. Four new HIV-1 group N isolates from Cameroon: prevalence continues to be low. AIDS Res Hum Retroviruses 26:109–115. https://doi.org/10.1089/aid.2009.0178.
19. Ayouba A, Souquieres S, Njinku B, Martin PM, Muller-Trutwin MC, Roques P, Barre-Sinoussi F, Mauclere P, Simon F, Nerrienet E. 2000. HIV-1 group N among HIV-1-seropositive individuals in Cameroon. AIDS 14:2623–2625. https://doi.org/10.1097/00002030-200011100-00033.
20. Malim MH, Emerman M. 2008. HIV-1 accessory proteins—ensuring viral survival in a hostile environment. Cell Host Microbe 3:388–398. https://doi.org/10.1016/j.chom.2008.04.008.
21. Sheehy AM, Gaddis NC, Choi JD, Malim MH. 2002. Isolation of a human gene that inhibits HIV-1 infection and is suppressed by the viral Vif protein. Nature 418:646–650. https://doi.org/10.1038/nature00939.
22. Neil SJ, Zang T, Bieniasz PD. 2008. Tetherin inhibits retrovirus release and is antagonized by HIV-1 Vpu. Nature 451:425–430. https://doi.org/10.1038/nature06553.
23. Van Damme N, Goff D, Katsura C, Jorgenson RL, Mitchell R, Johnson MC, Stephens EB, Guatelli J. 2008. The interferon-induced protein BST-2 restricts HIV-1 release and is downregulated from the cell surface by the viral Vpu protein. Cell Host Microbe 3:245–252. https://doi.org/10.1016/j.chom.2008.03.001.
24. Evans DT, Serra-Moreno R, Singh RK, Guatelli JC. 2010. BST-2/tetherin: a new component of the innate immune response to enveloped viruses. Trends Microbiol 18:388–396. https://doi.org/10.1016/j.tim.2010.06.010.
25. Kirchhoff F. 2010. Immune evasion and counteraction of restriction factors by HIV-1 and other primate lentiviruses. Cell Host Microbe 8:55–67. https://doi.org/10.1016/j.chom.2010.06.004.
26. Malim MH. 2009. APOBEC proteins and intrinsic resistance to HIV-1 infection. Philos Trans R Soc Lond B Biol Sci 364:675–687. https://doi.org/10.1098/rstb.2008.0185.
27. Soper A, Juarez-Fernandez G, Aso H, Moriwaki M, Yamada E, Nakano Y, Koyanagi Y, Sato K. 2017. Various plus unique: viral protein U as a plurifunctional protein for HIV-1 replication. Exp Biol Med (Maywood) 242:850–858. https://doi.org/10.1177/1535370217697384.
28. Kluge SF, Sauter D, Vogl M, Peeters M, Li Y, Bibollet-Ruche F, Hahn BH, Kirchhoff F. 2013. The transmembrane domain of HIV-1 Vpu is sufficient to confer anti-tetherin activity to SIVcpz and SIVgor Vpu proteins: cytoplasmic determinants of Vpu function. Retrovirology 10:32. https://doi.org/10.1186/1742-4690-10-32.
29. Sauter D, Schindler M, Specht A, Landford WN, Munch J, Kim KA, Votteler J, Schubert U, Bibollet-Ruche F, Keele BF, Takehisa J, Ogando Y, Ochsenbauer C, Kappes JC, Ayouba A, Peeters M, Learn GH, Shaw G, Sharp PM, Bieniasz P, Hahn BH, Hatziioannou T, Kirchhoff F. 2009. Tetherin-driven adaptation of Vpu and Nef function and the evolution of pandemic and nonpandemic HIV-1 strains. Cell Host Microbe 6:409–421. https://doi.org/10.1016/j.chom.2009.10.004.
30. Yang SJ, Lopez LA, Exline CM, Haworth KG, Cannon PM. 2011. Lack of adaptation to human tetherin in HIV-1 group O and P. Retrovirology 8:78. https://doi.org/10.1186/1742-4690-8-78.
31. Iwami S, Sato K, Morita S, Inaba H, Kobayashi T, Takeuchi JS, Kimura Y, Misawa N, Ren F, Iwasa Y, Aihara K, Koyanagi Y. 2015. Pandemic HIV-1 Vpu overcomes intrinsic herd immunity mediated by tetherin. Sci Rep 5:12256. https://doi.org/10.1038/srep12256.
32. Bibollet-Ruche F, Heigele A, Keele BF, Easlick JL, Decker JM, Takehisa J, Learn G, Sharp PM, Hahn BH, Kirchhoff F. 2012. Efficient SIVcpz replication in human lymphoid tissue requires viral matrix protein adaptation. J Clin Invest 122:1644–1652. https://doi.org/10.1172/JCI61429.
33. Yuan Z, Kang G, Ma F, Lu W, Fan W, Fennessey CM, Keele BF, Li Q. 2016. Recapitulating cross-species transmission of simian immunodeficiency virus SIVcpz to humans by using humanized BLT mice. J Virol 90:7728–7739. https://doi.org/10.1128/JVI.00860-16.
34. Nie C, Sato K, Misawa N, Kitayama H, Fujino H, Hiramatsu H, Heike T, Nakahata T, Tanaka Y, Ito M, Koyanagi Y. 2009. Selective infection of $CD4^+$ effector memory T lymphocytes leads to preferential depletion of memory T lymphocytes in R5 HIV-1-infected humanized NOD/SCID/IL-2Rgnull mice. Virology 394:64–72. https://doi.org/10.1016/j.virol.2009.08.011.
35. Sato K, Koyanagi Y. 2011. The mouse is out of the bag: insights and perspectives on HIV-1-infected humanized mouse models. Exp Biol Med 236:977–985. https://doi.org/10.1258/ebm.2011.010294.
36. Sato K, Nie C, Misawa N, Tanaka Y, Ito M, Koyanagi Y. 2010. Dynamics of memory and naive $CD8^+$ T lymphocytes in humanized NOD/SCID/IL-2Rgammanull mice infected with CCR5-tropic HIV-1. Vaccine 28(Suppl 2):B32–B37. https://doi.org/10.1016/j.vaccine.2009.10.154.
37. Nakano Y, Misawa N, Juarez-Fernandez G, Moriwaki M, Nakaoka S, Funo T, Yamada E, Soper A, Yoshikawa R, Ebrahimi D, Tachiki Y, Iwami S, Harris RS, Koyanagi Y, Sato K. 2017. HIV-1 competition experiments in humanized mice show that APOBEC3H imposes selective pressure and promotes virus adaptation. PLoS Pathog 13:e1006348. https://doi.org/10.1371/journal.ppat.1006348.
38. Sato K, Izumi T, Misawa N, Kobayashi T, Yamashita Y, Ohmichi M, Ito M, Takaori-Kondo A, Koyanagi Y. 2010. Remarkable lethal G-to-A mutations in vif-proficient HIV-1 provirus by individual APOBEC3 proteins in humanized mice. J Virol 84:9546–9556. https://doi.org/10.1128/JVI.00823-10.
39. Sato K, Misawa N, Fukuhara M, Iwami S, An DS, Ito M, Koyanagi Y. 2012. Vpu augments the initial burst phase of HIV-1 propagation and downregulates BST2 and CD4 in humanized mice. J Virol 86:5000–5013. https://doi.org/10.1128/JVI.07062-11.
40. Sato K, Misawa N, Iwami S, Satou Y, Matsuoka M, Ishizaka Y, Ito M, Aihara K, An DS, Koyanagi Y. 2013. HIV-1 Vpr accelerates viral replication during acute infection by exploitation of proliferating $CD4^+$ T cells *in vivo*. PLoS Pathog 9:e1003812. https://doi.org/10.1371/journal.ppat.1003812.
41. Sato K, Takeuchi JS, Misawa N, Izumi T, Kobayashi T, Kimura Y, Iwami S, Takaori-Kondo A, Hu WS, Aihara K, Ito M, An DS, Pathak VK, Koyanagi Y. 2014. APOBEC3D and APOBEC3F potently promote HIV-1 diversification and evolution in humanized mouse model. PLoS Pathog 10:e1004453. https://doi.org/10.1371/journal.ppat.1004453.
42. Yamada E, Yoshikawa R, Nakano Y, Misawa N, Koyanagi Y, Sato K. 2015. Impacts of humanized mouse models on the investigation of HIV-1 infection: illuminating the roles of viral accessory proteins in vivo. Viruses 7:1373–1390. https://doi.org/10.3390/v7031373.
43. Wain LV, Bailes E, Bibollet-Ruche F, Decker JM, Keele BF, Van Heuverswyn F, Li Y, Takehisa J, Ngole EM, Shaw GM, Peeters M, Hahn BH, Sharp PM. 2007. Adaptation of HIV-1 to its human host. Mol Biol Evol 24:1853–1860. https://doi.org/10.1093/molbev/msm110.
44. D'Arc M, Ayouba A, Esteban A, Learn GH, Boue V, Liegeois F, Etienne L, Tagg N, Leendertz FH, Boesch C, Madinda NF, Robbins MM, Gray M,

Cournil A, Ooms M, Letko M, Simon VA, Sharp PM, Hahn BH, Delaporte E, Mpoudi Ngole E, Peeters M. 2015. Origin of the HIV-1 group O epidemic in western lowland gorillas. Proc Natl Acad Sci U S A 112:E1343–E1352. https://doi.org/10.1073/pnas.1502022112.
45. Etienne L, Hahn BH, Sharp PM, Matsen FA, Emerman M. 2013. Gene loss and adaptation to hominids underlie the ancient origin of HIV-1. Cell Host Microbe 14:85–92. https://doi.org/10.1016/j.chom.2013.06.002.
46. Letko M, Silvestri G, Hahn BH, Bibollet-Ruche F, Gokcumen O, Simon V, Ooms M. 2013. Vif proteins from diverse primate lentiviral lineages use the same binding site in APOBEC3G. J Virol 87:11861–11871. https://doi.org/10.1128/JVI.01944-13.
47. Ikeda H, Nakaoka S, de Boer RJ, Morita S, Misawa N, Koyanagi Y, Aihara K, Sato K, Iwami S. 2016. Quantifying the effect of Vpu on the promotion of HIV-1 replication in the humanized mouse model. Retrovirology 13:23. https://doi.org/10.1186/s12977-016-0252-2.
48. Gilden RV, Arthur LO, Robey WG, Kelliher JC, Graham CE, Fischinger PJ. 1986. HTLV-III antibody in a breeding chimpanzee not experimentally exposed to the virus. Lancet i:678–679.
49. Greenwood EJ, Schmidt F, Kondova I, Niphuis H, Hodara VL, Clissold L, McLay K, Guerra B, Redrobe S, Giavedoni LD, Lanford RE, Murthy KK, Rouet F, Heeney JL. 2015. Simian immunodeficiency virus infection of chimpanzees (Pan troglodytes) shares features of both pathogenic and non-pathogenic lentiviral infections. PLoS Pathog 11:e1005146. https://doi.org/10.1371/journal.ppat.1005146.
50. Keele BF, Jones JH, Terio KA, Estes JD, Rudicell RS, Wilson ML, Li Y, Learn GH, Beasley TM, Schumacher-Stankey J, Wroblewski E, Mosser A, Raphael J, Kamenya S, Lonsdorf EV, Travis DA, Mlengeya T, Kinsel MJ, Else JG, Silvestri G, Goodall J, Sharp PM, Shaw GM, Pusey AE, Hahn BH. 2009. Increased mortality and AIDS-like immunopathology in wild chimpanzees infected with SIVcpz. Nature 460:515–519. https://doi.org/10.1038/nature08200.
51. Gao F, Bailes E, Robertson DL, Chen Y, Rodenburg CM, Michael SF, Cummins LB, Arthur LO, Peeters M, Shaw GM, Sharp PM, Hahn BH. 1999. Origin of HIV-1 in the chimpanzee Pan troglodytes troglodytes. Nature 397:436–441. https://doi.org/10.1038/17130.
52. Van Heuverswyn F, Li Y, Bailes E, Neel C, Lafay B, Keele BF, Shaw KS, Takehisa J, Kraus MH, Loul S, Butel C, Liegeois F, Yangda B, Sharp PM, Mpoudi-Ngole E, Delaporte E, Hahn BH, Peeters M. 2007. Genetic diversity and phylogeographic clustering of SIVcpzPtt in wild chimpanzees in Cameroon. Virology 368:155–171. https://doi.org/10.1016/j.virol.2007.06.018.
53. Sharp PM, Hahn BH. 2010. The evolution of HIV-1 and the origin of AIDS. Philos Trans R Soc Lond B Biol Sci 365:2487–2494. https://doi.org/10.1098/rstb.2010.0031.
54. Takehisa J, Kraus MH, Ayouba A, Bailes E, Van Heuverswyn F, Decker JM, Li Y, Rudicell RS, Learn GH, Neel C, Ngole EM, Shaw GM, Peeters M, Sharp PM, Hahn BH. 2009. Origin and biology of simian immunodeficiency virus in wild-living western gorillas. J Virol 83:1635–1648. https://doi.org/10.1128/JVI.02311-08.
55. Simon F, Mauclere P, Roques P, Loussert-Ajaka I, Muller-Trutwin MC, Saragosti S, Georges-Courbot MC, Barre-Sinoussi F, Brun-Vezinet F. 1998. Identification of a new human immunodeficiency virus type 1 distinct from group M and group O. Nat Med 4:1032–1037. https://doi.org/10.1038/2017.
56. Roques P, Robertson DL, Souquiere S, Apetrei C, Nerrienet E, Barre-Sinoussi F, Muller-Trutwin M, Simon F. 2004. Phylogenetic characteristics of three new HIV-1 N strains and implications for the origin of group N. AIDS 18:1371–1381. https://doi.org/10.1097/01.aids.0000125990.86904.28.
57. Sauter D, Unterweger D, Vogl M, Usmani SM, Heigele A, Kluge SF, Hermkes E, Moll M, Barker E, Peeters M, Learn GH, Bibollet-Ruche F, Fritz JV, Fackler OT, Hahn BH, Kirchhoff F. 2012. Human tetherin exerts strong selection pressure on the HIV-1 group N Vpu protein. PLoS Pathog 8:e1003093. https://doi.org/10.1371/journal.ppat.1003093.
58. Kirchhoff F, Schindler M, Bailer N, Renkema GH, Saksela K, Knoop V, Muller-Trutwin MC, Santiago ML, Bibollet-Ruche F, Dittmar MT, Heeney JL, Hahn BH, Munch J. 2004. Nef proteins from simian immunodeficiency virus-infected chimpanzees interact with p21-activated kinase 2 and modulate cell surface expression of various human receptors. J Virol 78:6864–6874. https://doi.org/10.1128/JVI.78.13.6864-6874.2004.
59. Delaugerre C, De Oliveira F, Lascoux-Combe C, Plantier JC, Simon F. 2011. HIV-1 group N: travelling beyond Cameroon. Lancet 378:1894. https://doi.org/10.1016/S0140-6736(11)61457-8.
60. Mwaengo DM, Novembre FJ. 1998. Molecular cloning and characterization of viruses isolated from chimpanzees with pathogenic human immunodeficiency virus type 1 infections. J Virol 72:8976–8987.
61. Gaddis NC, Sheehy AM, Ahmad KM, Swanson CM, Bishop KN, Beer BE, Marx PA, Gao F, Bibollet-Ruche F, Hahn BH, Malim MH. 2004. Further investigation of simian immunodeficiency virus Vif function in human cells. J Virol 78:12041–12046. https://doi.org/10.1128/JVI.78.21.12041-12046.2004.
62. Ministry of Education, Culture, Sports, Science, and Technology, Japan. 2006. Guidelines for the proper conduct of animal experiments. Ministry of Education, Culture, Sports, Science and Technology, Japan, Tokyo, Japan.
63. Ito M, Hiramatsu H, Kobayashi K, Suzue K, Kawahata M, Hioki K, Ueyama Y, Koyanagi Y, Sugamura K, Tsuji K, Heike T, Nakahata T. 2002. NOD/SCID/gcnull mouse: an excellent recipient mouse model for engraftment of human cells. Blood 100:3175–3182. https://doi.org/10.1182/blood-2001-12-0207.
64. An DS, Poon B, Ho Tsong Fang R, Weijer K, Blom B, Spits H, Chen IS, Uittenbogaart CH. 2007. Use of a novel chimeric mouse model with a functionally active human immune system to study human immunodeficiency virus type 1 infection. Clin Vaccine Immunol 14:391–396. https://doi.org/10.1128/CVI.00403-06.
65. Sato K, Misawa N, Nie C, Satou Y, Iwakiri D, Matsuoka M, Takahashi R, Kuzushima K, Ito M, Takada K, Koyanagi Y. 2011. A novel animal model of Epstein-Barr virus-associated hemophagocytic lymphohistiocytosis in humanized mice. Blood 117:5663–5673. https://doi.org/10.1182/blood-2010-09-305979.
66. Wei X, Decker JM, Liu H, Zhang Z, Arani RB, Kilby JM, Saag MS, Wu X, Shaw GM, Kappes JC. 2002. Emergence of resistant human immunodeficiency virus type 1 in patients receiving fusion inhibitor (T-20) monotherapy. Antimicrob Agents Chemother 46:1896–1905. https://doi.org/10.1128/AAC.46.6.1896-1905.2002.
67. Sato K, Aoki J, Misawa N, Daikoku E, Sano K, Tanaka Y, Koyanagi Y. 2008. Modulation of human immunodeficiency virus type 1 infectivity through incorporation of tetraspanin proteins. J Virol 82:1021–1033. https://doi.org/10.1128/JVI.01044-07.
68. Tamura K, Peterson D, Peterson N, Stecher G, Nei M, Kumar S. 2011. MEGA5: molecular evolutionary genetics analysis using maximum likelihood, evolutionary distance, and maximum parsimony methods. Mol Biol Evol 28:2731–2739. https://doi.org/10.1093/molbev/msr121.
69. Guindon S, Dufayard JF, Lefort V, Anisimova M, Hordijk W, Gascuel O. 2010. New algorithms and methods to estimate maximum-likelihood phylogenies: assessing the performance of PhyML 3.0. Syst Biol 59:307–321. https://doi.org/10.1093/sysbio/syq010.
70. Adachi A, Gendelman HE, Koenig S, Folks T, Willey R, Rabson A, Martin MA. 1986. Production of acquired immunodeficiency syndrome-associated retrovirus in human and nonhuman cells transfected with an infectious molecular clone. J Virol 59:284–291.
71. Suzuki Y, Koyanagi Y, Tanaka Y, Murakami T, Misawa N, Maeda N, Kimura T, Shida H, Hoxie JA, O'Brien WA, Yamamoto N. 1999. Determinant in human immunodeficiency virus type 1 for efficient replication under cytokine-induced $CD4^+$ T-helper 1 (Th1)- and Th2-type conditions. J Virol 73:316–324.
72. Koyanagi Y, Miles S, Mitsuyasu RT, Merrill JE, Vinters HV, Chen IS. 1987. Dual infection of the central nervous system by AIDS viruses with distinct cellular tropisms. Science 236:819–822. https://doi.org/10.1126/science.3646751.
73. Theodore TS, Englund G, Buckler-White A, Buckler CE, Martin MA, Peden KW. 1996. Construction and characterization of a stable full-length macrophage-tropic HIV type 1 molecular clone that directs the production of high titers of progeny virions. AIDS Res Hum Retroviruses 12:191–194. https://doi.org/10.1089/aid.1996.12.191.
74. Arnold K, Bordoli L, Kopp J, Schwede T. 2006. The SWISS-MODEL workspace: a web-based environment for protein structure homology modelling. Bioinformatics 22:195–201. https://doi.org/10.1093/bioinformatics/bti770.
75. Biasini M, Bienert S, Waterhouse A, Arnold K, Studer G, Schmidt T, Kiefer F, Gallo Cassarino T, Bertoni M, Bordoli L, Schwede T. 2014. SWISS-MODEL: modelling protein tertiary and quaternary structure using evolutionary information. Nucleic Acids Res 42:W252–W258. https://doi.org/10.1093/nar/gku340.
76. Guex N, Peitsch MC, Schwede T. 2009. Automated comparative protein structure modeling with SWISS-MODEL and Swiss-PdbViewer: a historical perspective. Electrophoresis 30(Suppl 1):S162–S173. https://doi.org/10.1002/elps.200900140.
77. Kiefer F, Arnold K, Kunzli M, Bordoli L, Schwede T. 2009. The SWISS-

MODEL Repository and associated resources. Nucleic Acids Res 37: D387–D392. https://doi.org/10.1093/nar/gkn750.
78. Zhou T, Zhu J, Wu X, Moquin S, Zhang B, Acharya P, Georgiev IS, Altae-Tran HR, Chuang GY, Joyce MG, Kwon YD, Longo NS, Louder MK, Luongo T, McKee K, Schramm CA, Skinner J, Yang Y, Yang Z, Zhang Z, Zheng A, Bonsignori M, Haynes BF, Scheid JF, Nussenzweig MC, Simek M, Burton DR, Koff WC, Program NCS, Mullikin JC, Connors M, Shapiro L, Nabel GJ, Mascola JR, Kwong PD. 2013. Multidonor analysis reveals structural elements, genetic determinants, and maturation pathway for HIV-1 neutralization by VRC01-class antibodies. Immunity 39:245–258. https://doi.org/10.1016/j.immuni.2013.04.012.
79. Xu D, Zhang Y. 2011. Improving the physical realism and structural accuracy of protein models by a two-step atomic-level energy minimization. Biophys J 101:2525–2534. https://doi.org/10.1016/j.bpj.2011.10.024.